

Influence of low frequency modes on dynamical concertedness in double proton transfer dynamics

Priyanka Pandey

*Department of Chemistry, Indian Institute of Technology
Kanpur, Uttar Pradesh 208016, India*

Shibabrat Naik

*School of Mathematics, University of Bristol
Fry Building, Woodland Road, Bristol BS8 1UG, United Kingdom*

Srihari Keshavamurthy

*Department of Chemistry, Indian Institute of Technology
Kanpur, Uttar Pradesh 208016, India*

Abstract

We analyze the classical phase space dynamics of a three degree of freedom Hamiltonian that models multiple bond breaking and forming reactions. The model Hamiltonian, inspired from studies on double proton transfer reactions, allows for exploring the dynamical consequences of higher index saddles on multidimensional potential energy surfaces. Studies have shown that coupling of low frequency transverse modes to the reaction coordinate can significantly influence the reaction mechanism, concerted or sequential, as inferred from a reduced dimensional analysis. Using the notion of dynamically concerted and sequential pathways, we provide insights into the role of the transverse modes by studying the delay times between the formation of two bonds. The delay time distribution, used extensively in earlier studies, is placed on a firm dynamical footing by correlating it with the phase space manifolds, determined using the technique of Lagrangian descriptors. We establish the utility of Lagrangian descriptors in identifying the phase space manifolds responsible for the dynamically concerted and dynamically sequential pathways.

Keywords: Double proton transfer, Sequential and concerted mechanisms, Delay time distributions, Lagrangian descriptor, Phase space structures, Higher index saddles

1. Introduction

The theory of nonlinear dynamical systems is a natural framework for understanding chemical reactions. There are several reasons for such a claim, but two of them are key. Firstly, breaking of a bond is only possible if the vibrations are modeled as nonlinear oscillators. Secondly, the canonical paradigm of associating an energized molecule with many such nonlinear oscillators that are coupled together [1–4] leads to a rich and complex dynamical behaviour that necessitates a phase space perspective for proper analysis

Email addresses: priyanka@iitk.ac.in (Priyanka Pandey), s.naik@bristol.ac.uk (Shibabrat Naik), srihari@iitk.ac.in (Srihari Keshavamurthy)

7 and interpretation [5, 6]. Indeed the central notion of a transition state is best understood as a dynamical
8 bottleneck that is formed by certain invariant manifolds in the phase space [7–13]. Reaction rates can then
9 be associated with fluxes through appropriate bottlenecks [14–16]. Thus, a local dynamical perspective on
10 Transition state theory (TST) has provided fresh insights into the usefulness and limitations of TST in the
11 microcanonical [17], canonical [18] and more general [19–23] settings.

12 Apart from the rates, there is yet another important aspect of a chemical reaction that is enshrined
13 in the TS - the mechanism. In fact, identifying the correct TS is essentially equivalent to a knowledge
14 of the mechanism of the reaction. For reactions involving a single TS (elementary reactions) one therefore
15 associates a single mechanism that leads to the transformation of the reactants to products. However, several
16 reactions are associated with potential energy surface (PES) that exhibit novel features [24] like extended flat
17 regions (calderas or more generally entropic intermediates), ambimodal TS, valley ridge inflection points,
18 several distinct saddle points (multiple TSs), and saddle points with more than one unstable direction (higher
19 index saddles). It is now clear that the existence of such features on the PES can lead to significant dynamical
20 effects. Examples include dynamical matching [25–30], nonstatistical branching ratios [31–33], energy
21 dependent product selectivity [34–36], and switching of reaction mechanisms [37–39]. Consequently, there
22 is an increased focus now on trajectory-based analysis of complex reactions.

23 In the current work we are interested in understanding the dynamics of reactions that involve breaking
24 and forming of multiple bonds. Here one invariably has to face up to a fundamental and essential mechanis-
25 tic question: is the process occurring sequentially or in a concerted fashion? In this regard, the Diels-Alder
26 and the double proton transfer (DPT) reactions have provided a rich arena to explore the role of dynamics
27 in determining the correct reaction mechanism [39–48]. From a fundamental point of view the possibility
28 of more than one distinct pathway is linked with the presence of several distinct TSs. Although tradition-
29 ally one associates TS with a index-1 saddle point on the multidimensional PES, several studies indicate
30 that the dynamical influence of higher index saddles on the PES can also be a deciding factor in identify-
31 ing the dominant mechanism [49–53]. For instance, for energies above the index-2 saddle one can have a
32 time-dependent switching between the concerted and sequential pathways. Recently, it was shown [37] that
33 such a dynamical mechanism switch is an inherently classical phenomenon. Moreover, owing to the mixed
34 regular-chaotic nature of the classical phase space, initial quantum wavepackets that are centered at specific
35 regions of the classical phase space can undergo strikingly different mechanism-switching dynamics [37].
36 Interestingly, the switching timescale is typically of the order of a bond stretching time period and hence
37 ultrafast. These observations therefore raise questions on the utility of a purely non-dynamical classification
38 of the mechanism as concerted or sequential. Such concerns have been raised by Carpenter in his early work
39 on the dynamic matching phenomenon wherein he emphasizes the “hazards associated with partitioning of
40 mechanisms into stepwise and concerted categories” based purely on the features on the static potential
41 energy surface [26]. More recently, Houk and coworkers introduced quantitative measures for classifying
42 the mechanism as dynamically concerted or sequential. Thus, for a given trajectory, if the time delay be-
43 tween the formation of the first bond and the second is shorter than a specified timescale then that particular
44 trajectory is classified as dynamically concerted [43]. As a consequence the central quantity of interest
45 is the distribution of the delay times associated with an appropriate ensemble of trajectories. Depending
46 on the nature of the delay time distributions one can identify the mechanism as dynamically concerted or
47 sequential.

48 Note that the approach of Houk and coworkers [43] implicitly invokes the dynamics in the full classical
49 phase space. Understandably, a detailed phase space analysis of the ab initio molecular dynamics based
50 studies of reactions like the Diels-Alder is far from easy. At the same time, there is no denying the fact
51 that rationalizing the dynamics based on the phase space structures is expected to yield rich dividends in

52 terms of our ability to predict rather than simply observe or compute. Thus, from a nonlinear dynamical
53 systems point of view it is natural to expect that the delay time distributions are intimately linked to the
54 disposition of the stable and unstable phase space manifolds that lead to transport from the reactant to
55 the product regions. However, identifying, let alone computing, such manifolds in very high dimensions
56 is not feasible at the present moment. A crucial question then is this: can reduced dimensional models
57 capture enough of the essential dynamics to allow for at least qualitative predictions? The answer, as
58 apparent from the several studies utilizing “minimal” models, is yes. For example, significant dynamical
59 insights into the phenomenon of roaming and dynamic matching have come from phase space studies on
60 the low dimensional model systems [25–29, 54–58]. Nevertheless, the detailed study of a electrocyclic ring
61 opening reaction by Kramer et al. highlights the central issues in this regard [59]. A comparison of the
62 direct dynamics calculations (in a 36-dimensional phase space) with the reduced two-dimensional model
63 dynamics for the same reaction revealed that the two do share dynamical similarities. However, they make
64 an important point - in the event that large amplitude modes, which would be considered as “spectator”
65 modes in the reduced dimensional treatment, couple to the reaction coordinate, the dynamics may be more
66 complicated than what would be predicted by the reduced dimensional models. Note that one can associate
67 large amplitude modes with low frequency vibrations and in a molecule with symmetry the various low
68 frequency modes can couple to the reactive mode in different ways due to the symmetry constraints. Thus,
69 apart from leading to a more complicated dynamics, can the coupling of specific low frequency modes alter
70 the inferred reduced dimensional mechanism itself?

71 Since the present study focuses on the DPT reaction in a specific class of molecules, we mention a few
72 examples from earlier studies that highlight the importance of the low frequency modes. In their extensive
73 review of multiple proton transfer dynamics, Smedarchina et al. [60] have argued for the importance of the
74 coupling of low frequency skeletal vibrations to the proton transfer modes. Furthermore, in a path integral
75 molecular dynamics simulation Yoshikawa et al. have shown that the low frequency out-of-plane vibration
76 can suppress the concerted pathway in porphycene molecule [61, 62]. Another example comes from the
77 Car-Parrinello molecular dynamics study of porphycene by Walewski et al., where it was observed that
78 excitations of selective low frequency modes, and combinations thereof, tend to enhance or suppress the
79 different mechanisms [63]. It is also relevant to point out the classical ab initio molecular dynamics study
80 of DPT by Ushiyama and Takatsuka where, apart from hints to the importance of delay time distributions,
81 the crucial role of skeletal vibrations to the second proton transfer was emphasized [45].

82 Clearly, and as discussed in detail in sec. 2, for a DPT reaction with two reactive modes, coupling of
83 even one low frequency transverse mode results in a system with three degrees of freedom. In this work
84 we investigate the classical dynamics of such a model system with the aim of explicitly correlating the
85 delay time distributions with the appropriate phase space manifolds. In particular, as mentioned above, we
86 investigate the influence on the delay time distributions due to the coupling of a third mode belonging to
87 a specific symmetry class. The results show that while high frequency modes do not significantly change
88 the fraction of concerted trajectories, the low frequency modes can substantially reduce the fraction. An
89 explanation of our delay time results in terms of the phase space structures is given by computing the
90 appropriate manifolds using the technique of Lagrangian descriptors(LD). We show that the the LD maps
91 faithfully capture the changes in the delay time distributions with varying coupling strength of the third
92 mode. In sec. 2 and Appendix A we motivate the model Hamiltonian used in our study. The influence
93 of the third mode on the delay time distributions are presented in sec. 3.3, followed by the results of the
94 delay time distributions for varying frequencies and coupling strengths. In sec. 3.4, aided by the stability
95 analysis of the linearized flow in Appendix B, the dynamical trajectory observations are correlated with
96 the LD-based determination of the relevant phase space manifolds. Finally, sec. 4 concludes with a brief

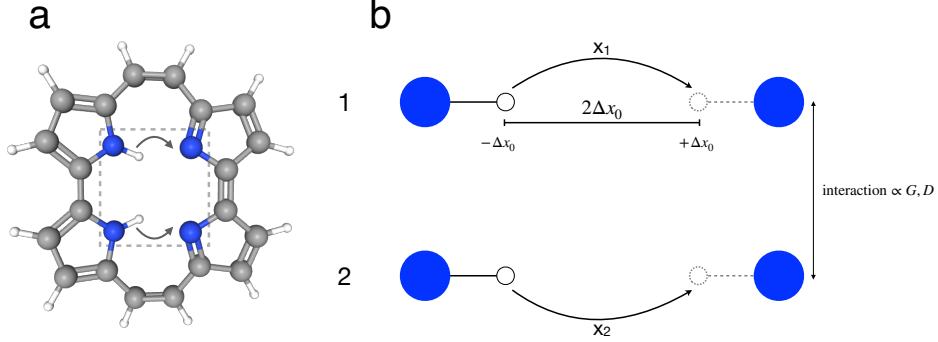
98 **2. Model Hamiltonian**

Figure 1: (a) The porphycene molecule with $N = 38$ atoms. The nitrogen, carbon, and hydrogen atoms are indicated in blue, grey, and white colors respectively. (b) Schematic for the double proton transfer model (indicated by arrows in both the panels) corresponding to the dashed square region shown in (a). The coordinates (x_1, x_2) correspond to the two proton transfer events. Each proton transfer subsystem is described by an appropriate double well potential with minima at $\pm\Delta x_0$. Interaction between the two subsystems is mediated by the coupling constant G and D at the leading order. See the main text and Appendix A for details.

To study the double proton transfer reaction, we consider a model three degree of freedom Hamiltonian motivated by the models introduced by Smedarchina et al. [64, 65] in their extensive studies. In Fig. 1 we show a schematic for the DPT process. The two proton transfer events occurring in the molecule (labeled as subsystem 1 and 2 in the figure) are described by one dimensional coordinates x_1 and x_2 with associated masses m_1 and m_2 , which are taken to be equal to the proton mass m_H . As shown in detail in Appendix A, an appropriate model two degrees of freedom dimensionless Hamiltonian for the coupled proton transfer is conveniently expressed in terms of the coordinates $(X_s, X_a) \equiv (\sqrt{M}x_s, \sqrt{M}x_a) = (\sqrt{M}(x_1 + x_2)/2, \sqrt{M}(x_1 - x_2)/2)$ with $M = m_1 + m_2 = 2m_H$. The Hamiltonian is of the form

$$H(\mathbf{X}, \mathbf{P}) = \frac{1}{2}(P_s^2 + P_a^2) + U(X_s, X_a) \quad (1)$$

with (P_s, P_a) being the momenta conjugate to (X_s, X_a) . The two dimensional potential energy surface is given by

$$U(\mathbf{X}) = \bar{\alpha}_s [X_s^2 - (\Delta X_s)^2]^2 + \bar{\alpha}_a [X_a^2 - (\Delta X_a)^2]^2 + 2\bar{R}X_s^2 X_a^2 + \mathcal{U}(G, D) \quad (2)$$

In the above we have denoted $(\mathbf{X}, \mathbf{P}) \equiv (X_s, X_a, P_s, P_a)$ with the parameters $\bar{\alpha}_s = \bar{\alpha}_a \equiv (1 - D)/M^2$ and $\bar{R} \equiv (3 + D)/M^2$. The various minima on the PES are given in terms of the quantities

$$\Delta X_{s,a} = \sqrt{\frac{M(1 \pm G)}{1 - D}} \quad (3)$$

and the constant energy shift is denoted as

$$\mathcal{U}(G, D) = 1 - \bar{\alpha}_s(\Delta X_s)^4 - \bar{\alpha}_a(\Delta X_a)^4 \quad (4)$$

99 The parameters G and D are specific to a given system (molecule) and correspond to the coupling of the two
100 proton transfer coordinates. We refer the reader to the Appendix A for a detailed derivation of the above

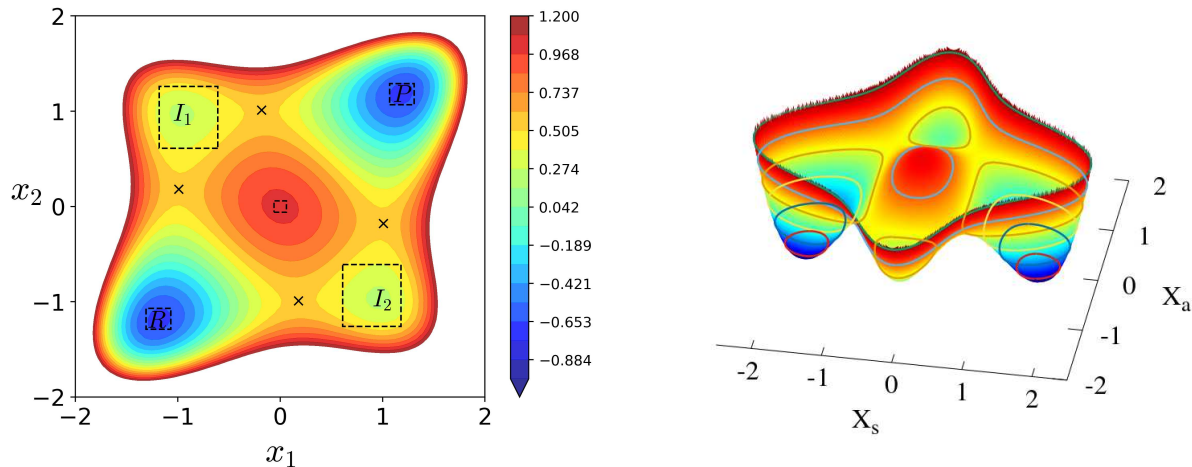


Figure 2: (Left panel) A contour plot of the model potential energy surface in the local (x_1, x_2) coordinates. (Right panel) A three dimensional plot of the potential energy surface in the mass-weighted (X_s, X_a) coordinates. The parameter values are $G = 0.2$, and $D = 0.15$. Different regions of the potential energy surface are shown inside the dotted space of the contour plot where R , P , and $I_{1,2}$ represent the reactant, product and intermediate regions respectively. The central box represents the index-2 saddle region. Note that the PES also exhibits four index-1 saddles, which are shown as \times .

101 Hamiltonian along with the relevant mass, length, and time scales. In Fig. 2 the two dimensional PES are
 102 shown in the two different sets of coordinates. Note that, in general, the number and type of critical points
 103 on the PES [65] depend on the values of G and D , mimicking a wide variety of dynamical systems. For the
 104 values of interest to us in the current work the PES exhibits a total of nine critical points which, as seen in
 105 Fig. 2, include four minima, four index-1 saddles and one index-2 saddle.

In the molecular context the Hamiltonian in Eqn. 1 captures the dynamics corresponding to the key reactive degrees of freedom. Thus, for an N -atom molecule of interest with $(3N - 6)$ vibrational degrees of freedom Eqn. 1 accounts for two of the degrees of freedom. However, the remaining $(3N - 8)$ modes that are transverse to the reactive modes typically do couple to the \mathbf{X} degrees of freedom to varying extents. Moreover, if the molecule of interest has a certain point group symmetry then the various transverse modes are constrained to couple to \mathbf{X} with specific functional form of the coupling potentials. For instance, in the context of DPT all the $(3N - 8)$ modes denoted by \mathbf{Y} couple at leading order via the potential

$$U_{\text{coup}}(\mathbf{X}, Y_k) = \frac{1}{2} \omega_{kY}^2 \left[Y_k - \frac{\lambda}{\omega_{kY}^2} g(\mathbf{X}) \right]^2 \quad (5)$$

106 with $g(\mathbf{X}) = X_{s,a}, X_s X_a$, and $X_{s,a}^2$ depending on the symmetry class to which the Y_k -mode belongs. In Eqn. 5
 107 the Y_k mode is modeled as a harmonic oscillator with the frequency of the mode denoted by ω_{kY} and λ
 108 being a measure of the coupling strength. It is interesting to note that with the above form of coupling
 109 one can still think of the \mathbf{Y} -modes as providing a “bath”, albeit a structured one. This is in contrast to the
 110 usual system-bath models wherein all the “bath” \mathbf{Y} -modes would couple bilinearly with a specified spectral
 111 density. Clearly, the dynamical implications of a structured and a non-structured bath are expected to be
 112 quite different for the reaction process.

113 As mentioned in the introduction, several studies have indicated the importance of including the ad-
 114 ditional modes since they can have a significant effect on the mechanism inferred from an analysis of the
 115 reduced dimensional Hamiltonian. Thus, certain symmetry modes tend to enhance a specific mechanism

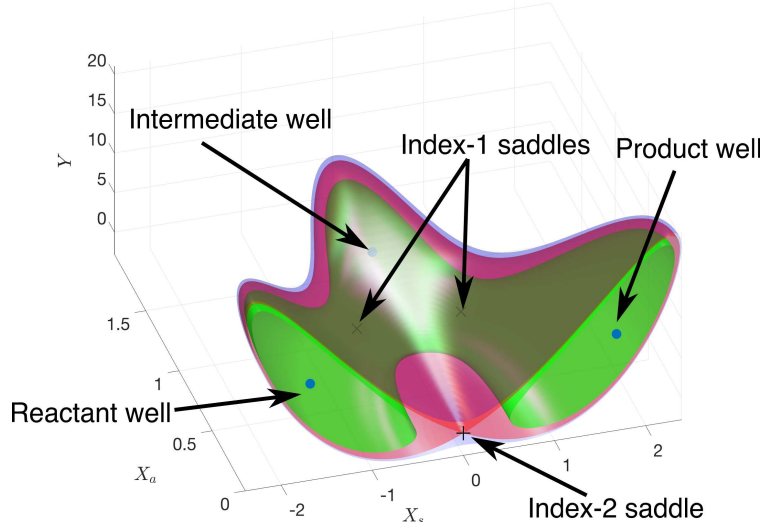


Figure 3: Potential energy visualized as equipotential surfaces for three energies. The green surface denotes $E < E_s$, red surface denotes $E = E_s$, and the blue surface denotes $E > E_s$. The energy of the index-2 saddle is E_s and denoted by the +, while the index-1 saddles are shown as \times . The parameter values are $G = 0.2$, $D = 0.15$, $\omega_Y = 0.3$, $\lambda = 0.3$ and $\lambda' = 0.1$ for the total energy, $E = 1.1$ to visualize the equipotential surfaces.

116 (concerted or sequential) whereas certain other symmetry modes act in an opposite manner [63]. Therefore,
 117 in order to rationalize the observed DPT rates one minimally needs to include two of the \mathbf{Y} -modes, resulting
 118 in a four degree of freedom Hamiltonian. However, understanding global phase space transport and linking
 119 it to the dynamical influence of the coupled \mathbf{Y} -modes in this case is a challenging task. Instead, here we ad-
 120 dress a simpler yet nontrivial question - can the coupling of a \mathbf{Y} -mode with a given symmetry significantly
 121 influence the reaction mechanism as inferred from the low dimensional system in Eqn. 1? And, if so, what
 122 is the dynamical origin of such a modulation? As noted above in Eqn. 5, there are several choices for the
 123 model Hamiltonian according to the $g(\mathbf{X})$ of interest. In this work we focus on the specific three degree of
 124 freedom Hamiltonian

$$H(\mathbf{X}, \mathbf{P}, Y, P_Y) = \frac{1}{2}(P_s^2 + P_a^2 + P_Y^2) + U(\mathbf{X}) + \frac{1}{2}\omega_Y^2 \left[Y - \frac{\lambda}{\omega_Y^2} X_s^2 - \frac{\lambda'}{\omega_Y^2} X_a^2 \right]^2 \quad (6)$$

$$\equiv \frac{1}{2}(P_s^2 + P_a^2 + P_Y^2) + V(\mathbf{X}, Y) \quad (7)$$

125 with $U(\mathbf{X})$ being the potential in Eqn. 2 and we continue to adopt the mass-weighted coordinate represen-
 126 tation. Note that the above form of coupling corresponds to the so called a_g -symmetry Y -mode and the
 127 importance of this coupling to DPT has been noted in several earlier studies. For example, in the $N = 38$
 128 atom porphycene molecule one has a total of $3N - 8 = 106$ \mathbf{Y} -modes. Among these modes the ones with a_g
 129 symmetry have substantial projection [66] onto the two reactive modes \mathbf{X} .

130 For the purpose of the current study we choose $0 < G < 1/2$ and $|D| < 2G$ which yields a total of nine
 131 critical points. The details associated with the critical points are given in Table 1. Note that there is no
 132 restriction on the sign of D . At the same time, for a given G , the dynamics corresponding to positive or
 133 negative D can be sufficiently different. For the rest of the paper we fix the values $G = 0.2$ and $D = 0.15$.
 134 Moreover, we fix the total energy at $E = 1.1$, which is slightly above the index-2 saddle energy (cf. Table 1).

135 Consequently, both the concerted and sequential pathways (examples can be seen in Fig. 4) from reactant to
 136 product are available classically. A key objective of the current study is to relate the phase space dynamics
 137 of the Hamiltonian in Eqn. 7 with the mechanism of DPT. In particular, we intend to assess the influence
 138 of the transverse Y -mode with both low and high frequencies ω_Y over a range of the couplings (λ, λ') . In
 139 Fig. 3 a representation of the PES $V(\mathbf{X}, Y)$ is shown for three values of the energy, $E < E_s, E = E_s, E > E_s$,
 140 where E_s is the energy of the index-2 saddle at the origin.

Configuration space coordinates	Total energy	Linear stability	Description
$\left(\pm\Delta X_s, 0, \frac{\lambda}{\omega_Y^2}(\Delta X_s)^2\right)$	$1 - \bar{\alpha}_s(\Delta X_s)^4$	C-C-C	reactant and product R, P
$\left(0, \pm\Delta X_a, \frac{\lambda'}{\omega_Y^2}(\Delta X_a)^2\right)$	$1 - \bar{\alpha}_a(\Delta X_a)^4$	C-C-C	intermediates $I_{1,2}$
$(X_s^\ddagger, X_a^\ddagger, Y^\ddagger)$	H^\ddagger	S-C-C	index-1 saddles
$(0, 0, 0)$	$E_s = 1$	S-S-C	index-2 saddle

Table 1: Equilibrium points, their respective energies and linear phase space stability. The stability types are denoted by C for center and S for saddle. For an explicit expression for $(X_s^\ddagger, X_a^\ddagger, Y^\ddagger)$ and the associated energy H^\ddagger see Appendix B.

141 3. Results and Discussions

142 3.1. Computational preliminaries: defining the initial ensemble, relevant regions, and delay time

143 In order to understand the influence of the (λ, λ') couplings and the frequency ω_Y of the transverse Y -
 144 mode on the dynamics of the Hamiltonian in Eqn. 7, we compute the delay time distribution. The concept
 145 of delay time distribution is motivated by the dynamical studies of Diels–Alder reactions by Houk and
 146 coworkers [43]. As the name suggests, the delay time corresponds to the time difference between the
 147 transfer of the first proton and the subsequent transfer of the second proton. By definition, the delay time
 148 is zero for a pure concerted pathway that proceeds directly from the reactant R to the product P via the
 149 index-2 saddle, and without visiting the intermediate regions. On the other hand, a sequential pathway
 150 from R to P via any or both the intermediate regions $I_{1,2}$ yields a finite value for the delay time. Therefore,
 151 demarcating different regions in the configuration space (i.e., reactant, intermediate, product, and index-2
 152 saddle) is necessary in order to compute the delay time and related measures. Consequently, in Fig. 2, the
 153 definitions of the various regions of the PES used in this study are shown as boxes of various sizes. We
 154 have divided the PES into five regions. The product and the reactant regions are centered at the minima
 155 $(\pm\Delta X_s, 0)$, and the region boundaries are at $(\pm 0.1\Delta X_s, \pm 0.15)$ from the minima. Similar regions are defined
 156 around the intermediate minima $(0, \pm\Delta X_a)$. However, for the intermediate regions, the region boundaries are
 157 at $(\pm 0.40, \pm 0.33\Delta X_a)$ from the minima. Since the height and the spread of the wells containing the global
 158 and local minima vary, therefore we are using different box sizes. The index-2 saddle region is centered at
 159 $(0, 0)$ with the boundaries at $(\pm 0.05, \pm 0.05)$. Note that there are other ways to assign the different regions
 160 on the PES and, naturally, the quantitative delay time distributions will be sensitive to the specific choice.
 161 However, within reasonable definitions of the regions, at a qualitative level the results are not expected to
 162 be significantly different i.e., the key trends with varying parameters are preserved.

163 For our calculations, we choose the initial values of position coordinates $X_s^{(0)}$ and $X_a^{(0)}$ randomly from
 164 the index-2 saddle region. This choice of the initial ensemble is to focus on the influence of the index-2
 165 saddle on the DPT. In addition, we randomly choose the initial momentum $P_s^{(0)} > 0$ and fix the initial value

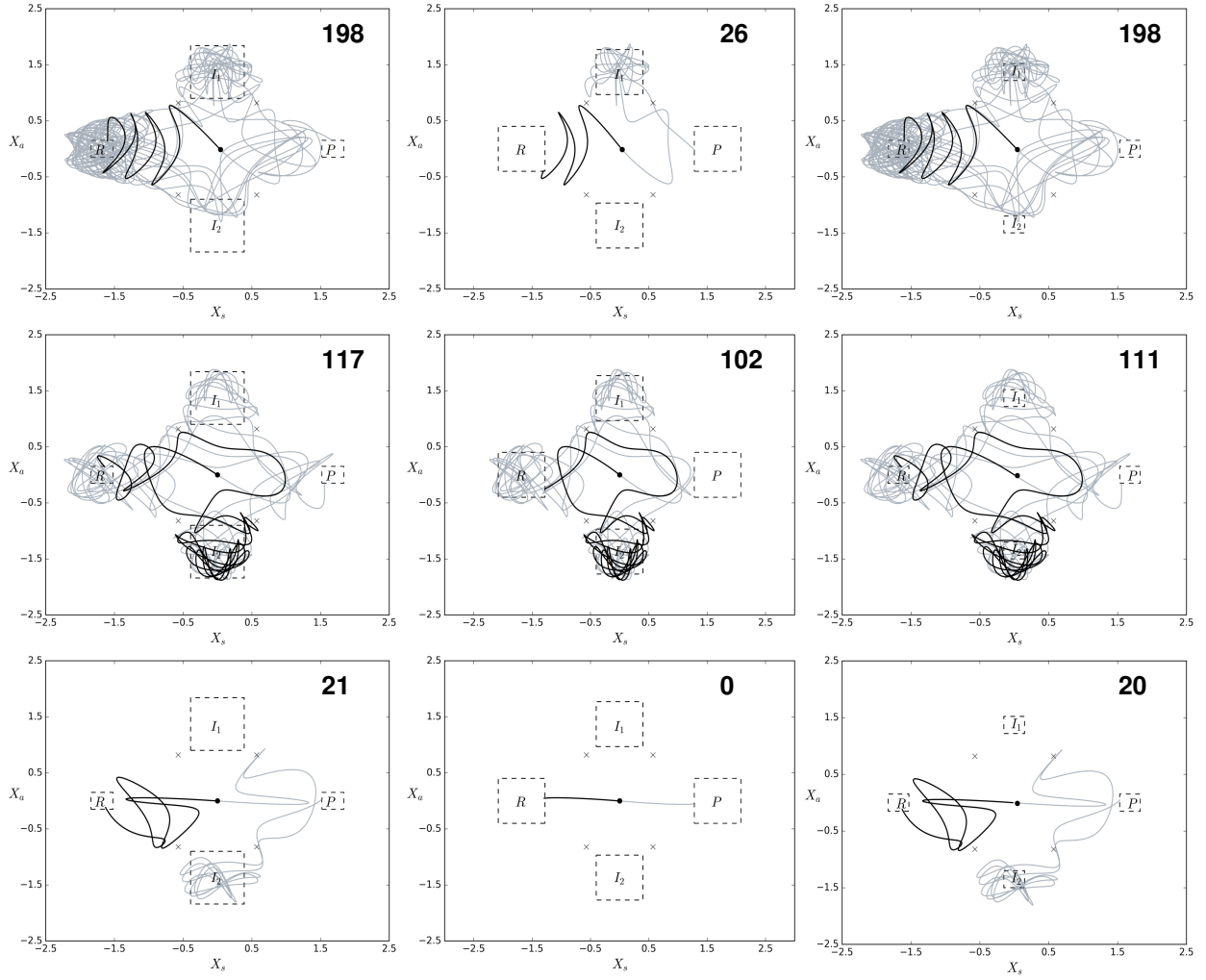


Figure 4: Examples trajectories with different delay times projected onto the (X_s, X_a) space. The various region definitions are shown as dashed boxes. (Left column) Region definitions used in the present work. (Middle column) Increased R and P region sizes. (Right column) Decreased I_1 and I_2 region sizes. All trajectories start at the index-2 saddle (solid circle) with a total energy $E = 1.1$. The forward and backward time propagation from the index-2 saddle are shown in grey and black respectively. The delay time assigned in each case is indicated in the respective panels. Note that the four index-1 saddles are indicated by \times . The example with zero delay time is a “pure” concerted trajectory.

166 of the third mode coordinate $Y^{(0)}$ and its conjugate momentum $P_Y^{(0)}$ at $(0, 0)$. Finally, the initial momentum
 167 $P_a^{(0)}$ is obtained by the energy conservation condition i.e., $H(\mathbf{X}^{(0)}, \mathbf{P}^{(0)}, Y^{(0)} = 0, P_Y^{(0)} = 0) = E = 1.1$.
 168 The specific total energy value, fixed for the rest of the study, corresponds to being just above the index-2
 169 saddle energy. Furthermore, note that the choice $P_s^{(0)} > 0$ corresponds to the trajectories at the index-2
 170 saddle having momentum in the direction of the product P . It is well known that the product selectivity
 171 of a chemical reaction in a trajectory calculation is strongly associated with the momentum distribution at
 172 the TS [25, 67]. Thus, although different initial momentum distributions at the index-2 saddle can lead
 173 to quantitatively different results, we believe that the qualitative insights are fairly robust. A total of 10^4
 174 trajectories were initiated from the index-2 saddle region and propagated both in the forward and backward
 175 direction until they reach the product and the reactant regions respectively. Trajectories, propagated up to
 176 a final time $t_f = 300$, are deemed to be reactive if they form the product in the forward direction and the
 177 reactant in the backward direction. Depending on the path a reactive trajectory takes and the associated
 178 delay time, we can characterize them as concerted or sequential trajectories. In Fig. 4 we show examples of
 179 a concerted and several sequential trajectories.

180 For the delay time computation we adopt the following strategy. The first instance when the forward
 181 time trajectory enters either of the intermediate regions $I_{1,2}$ is noted as t_I . This event corresponds to the
 182 transfer of either one of the proton (cf. Fig. 1). Subsequently, the time at which the trajectory enters the
 183 defined product region P is denoted as t_P . This time corresponds to the second proton transfer and hence
 184 $\Delta\tau = t_P - t_I$ is associated as the delay time for the specific trajectory. Two points are important to note at this
 185 stage. First, between t_I and t_P the trajectory may visit the reactant region R or visit the intermediate regions
 186 several times. Second, the $\Delta\tau$ as defined is sensitive to the extent of the different regions. Thus, variations
 187 in the region sizes can change the $\Delta\tau$ for a given trajectory. Examples for the same are shown in Fig. 4
 188 and it is clear that some of the large $\Delta\tau$ can become considerably smaller or a short $\Delta\tau$ sequential trajectory
 189 can turn into a concerted trajectory. However, the effect of such variations on the distribution $P(\Delta\tau)$ shown
 190 in Fig. 6 is not expected to be significant. In particular, the qualitative trends seen in Fig. 5 and Fig. 6 are
 191 robust to small variations in the region sizes.

192 3.2. Effect of the third degree of freedom on the concerted pathways

193 Before discussing our results for the delay time distributions, in Fig. 5 we show the influence of the third
 194 degree of freedom coupling in Eqn. 7 on the “pure” (as opposed to dynamically) concerted mechanism. In
 195 particular, Fig. 5(a) and (b) show the fraction of concerted trajectories f_{conc} upon coupling only the $X_s - Y$
 196 modes ($\lambda' = 0$) and the $X_a - Y$ modes ($\lambda = 0$) respectively. Note that the Hamiltonian in Eqn. 7 involves both
 197 the couplings and hence the results in Fig. 5(a) and (b) are a bit artificial. Nevertheless, such an analysis
 198 allows for dissecting, and a better understanding, of the results for the actual a_g -symmetry coupling form.
 199 It is clear from Fig. 5(a) that, apart from the initial oscillatory nature¹, low ω_Y tend to drastically reduce
 200 f_{conc} for increasing λ , while relatively larger ω_Y lead to a slight increase. On the other hand, the results
 201 in Fig. 5(b) indicate that f_{conc} increases moderately upon increasing the $X_a - Y$ mode coupling strengths.
 202 Therefore, the full a_g -symmetry coupling case with $\lambda, \lambda' \neq 0$ should encode the subtle competition between
 203 the two couplings. This is confirmed in Fig. 5(c) where, as an example, the variation in f_{conc} with λ' for
 204 a fixed value of $\lambda = 0.3$ is shown. Interestingly, now the high ω_Y cases show very little variation over a

¹We remark here that the f_{conc} in Fig. 5(a) exhibits peaks at certain values of $\lambda \equiv \lambda_p$. Interestingly, these peaks seem to occur when the reactant well harmonic frequencies $\omega_s(\lambda)$ and ω_a become degenerate. An approximate estimate is $\lambda_p \approx \omega_Y [(\omega_a/2\Delta X_s)^2 - 2\bar{\alpha}_s]^{1/2}$. For the parameters of interest, $\lambda_p \approx 0.47\omega_Y$. Note that the degeneracy is driven by the $X_s - Y$ coupling and hence an explicit three degrees of freedom effect. At the present moment we do not have a dynamical insight into this observation.

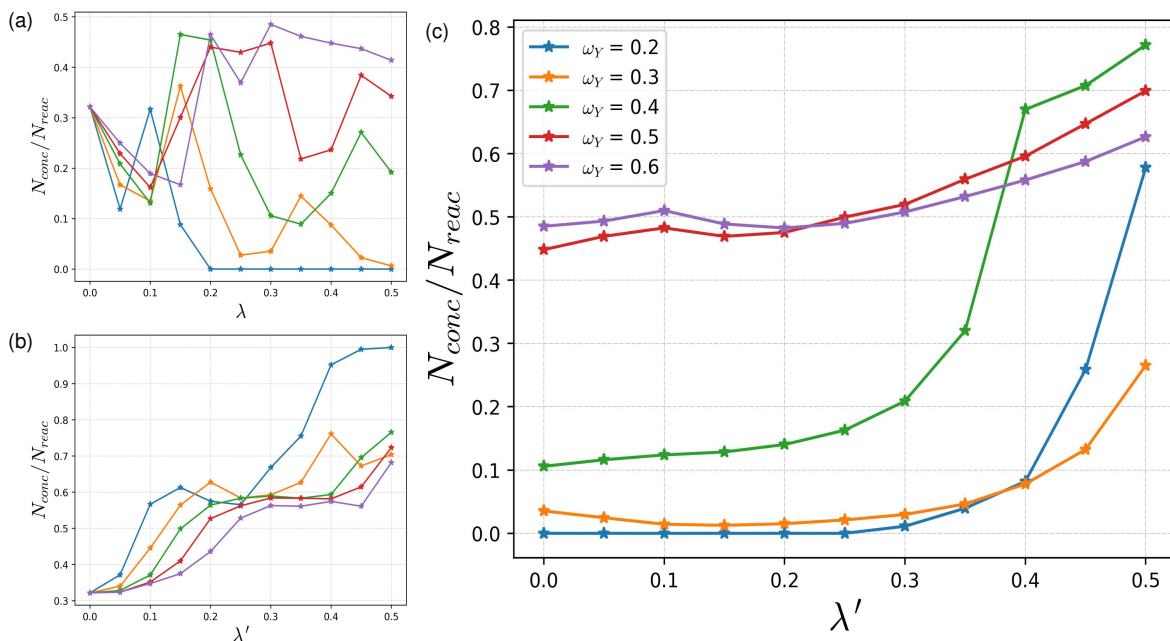


Figure 5: The fraction of concerted trajectories ($f_{conc} = N_{conc}/N_{reac}$) as a function of the coupling parameters. Here N_{reac} is the total number of reactive trajectories i.e., ones that start at the index-2 saddle and go to the product P and reactant R regions in forward and backward time propagation. The total integration time is $t_f = 300$. (a) Variation with λ for fixed $\lambda' = 0$ (b) Variation with λ' for fixed $\lambda = 0$ (c) Variation with λ' for fixed $\lambda = 0.3$. The frequency ω_Y of the transverse Y-mode are shown in the legend. It is important to note that N_{reac} varies with the $(\lambda, \lambda', \omega_Y)$ parameters.

205 significant range of the $X_a - Y$ coupling strengths. In contrast, for $\omega_Y \leq 0.4$ the results are more complex with
 206 f_{conc} increasing with λ' and the oscillations seen in Fig. 5(a) being absent. As expected, for $\lambda' > \lambda = 0.3$
 207 one observes f_{conc} increasing substantially. Nevertheless, it is evident from Fig. 5(c) that even for relatively
 208 large λ' values the $\omega_Y = 0.2$ and 0.3 cases have considerably lower f_{conc} in comparison to the uncoupled
 209 case. We remark that these results agree with the general expectation that coupling of the large amplitude
 210 (low frequency) modes to the reaction coordinate can lead to dynamical behaviours that are vastly different
 211 from the dynamics of reduced dimensional systems.

212 Note that Fig. 5 pertains to the pure concerted pathways and hence, by definition, zero delay times.
 213 Based on the discussions in the introduction, a useful perspective is to focus on the fraction of dynamically
 214 concerted trajectories. Thus, although Fig. 5 indicates that low values of ω_Y lead to a reduced f_{conc} , is it
 215 possible that most of the trajectories are still dynamically concerted for a reasonable choice for the delay
 216 time cutoff $\Delta\tau_c$. In other words, if the distribution of delay times $P(\Delta\tau)$ associated with the initial ensemble
 217 of trajectories in Fig. 5 is strongly peaked for $\Delta\tau \leq \Delta\tau_c$ then the mechanism would be labeled as dynamically
 218 concerted. Consequently, as argued by Black et al. [43], the significant lowering of f_{conc} for small ω_Y values
 219 observed in Fig. 5 need not really imply a major change in the reaction mechanism. Therefore, to ascertain
 220 if this indeed is the case we now turn our attention to the computation of the delay time distributions.

221 3.3. Delay time distributions: importance of the low frequency transverse modes

222 From the discussions above, it is clear that in order to analyze $P(\Delta\tau)$ results for our model system it is
 223 essential to define the cutoff $\Delta\tau_c$. One possible choice for this cutoff time is related to the lifetime of a TS
 224 according to the Eyring equation [68, 69]. This timescale is set by the prefactor of TST i.e., $\Delta\tau_c \sim h/k_B T$

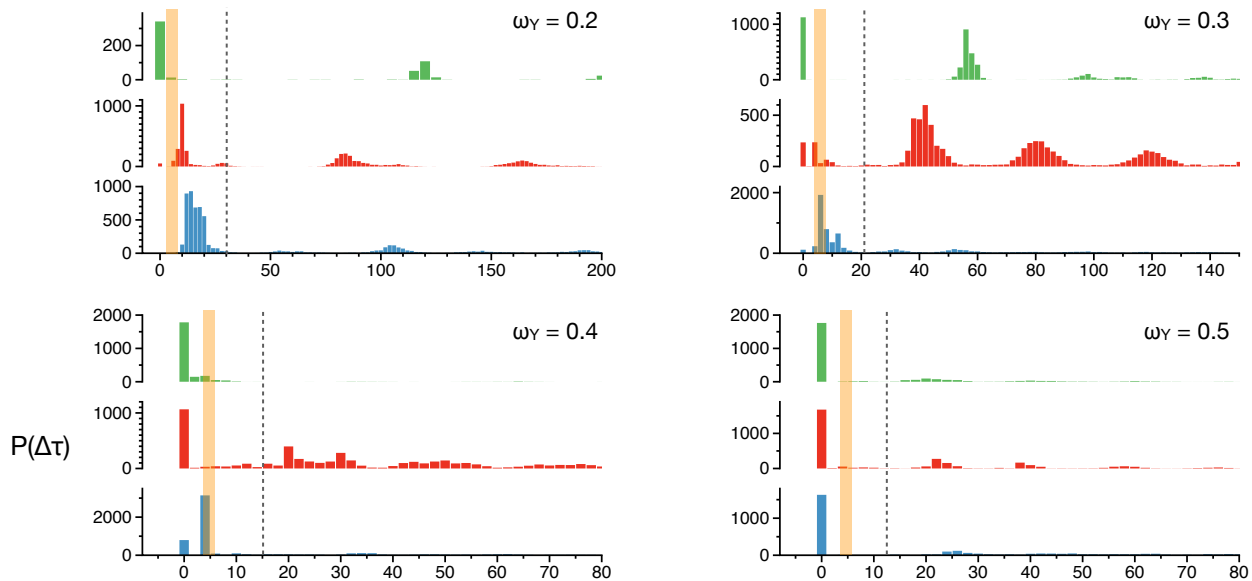


Figure 6: Delay time distributions $P(\Delta\tau)$ for fixed $\lambda = 0.3$ and varying λ' . The frequency ω_Y of the transverse Y-mode is indicated in each case. The histograms in blue, red, and green correspond to λ' value 0.1, 0.3 and 0.5 respectively. The orange vertical bar at $\Delta\tau_c \sim 5$ indicates the timescale associated with the unstable directions at the index-2 saddle. Note that the axis scales are different for each case and for comparison in each case the vertical dashed line corresponds to the harmonic period $2\pi/\omega_Y$ associated with the transverse mode.

225 with h , k_B , and T being the Planck constant, Boltzmann constant and temperature respectively. However, as
 226 we are dealing with a index-2 saddle and the dynamics is at zero temperature, we choose $\Delta\tau_c$ based on the
 227 timescales associated with the reactant oscillations [43] or the unstable motion at the index-2 saddle. Such
 228 criteria have been invoked before in several studies [70]. For our model system and parameters of interest,
 229 as shown in Appendix B, the unstable frequencies $\Omega_s^* \sim 1.6$ and $\Omega_a^* \sim 1.3$ at the index-2 saddle. These
 230 frequencies, independent of the couplings (λ, λ') due to the form of the Hamiltonian, translate roughly to a
 231 timescale $T_{s,a}^* \sim 5$. On the other hand, of the two harmonic frequencies around the reactant minimum, only
 232 Ω_s depends on (λ, ω_Y) and varies from ~ 5.5 ($\omega_Y = 0.2$) to ~ 3.0 ($\omega_Y = 0.5$), while $\Omega_a \sim 2.7$ stays fixed.
 233 Consequently, the harmonic timescales associated with the proton transfer modes at the reactant minimum
 234 is about $T_h \sim 2$. In this work, we therefore choose the conservative estimate $\Delta\tau_c \sim 5$ for discussing the
 235 delay time results.

236 The results of the delay time computations are shown in Fig. 6 for fixed $\lambda = 0.3$ as histograms². In
 237 each panel of Fig. 6 the transverse mode frequency ω_Y is fixed and the delay time distributions for three
 238 values of λ' are shown. Note that the both f_{conc} , shown in Fig. 5, and $P(\Delta\tau)$ are computed using same
 239 initial ensemble. In addition, the parameters used for generating Fig. 6 are fairly representative of other
 240 parameter sets as well. For the value of $\omega_Y = 0.4$ and 0.5 Fig. 6 (bottom panels) shows that a large fraction
 241 of the distribution is concentrated for $\Delta\tau \leq \Delta\tau_c$, implying that the mechanism is dynamically concerted.
 242 In contrast, for the case of $\omega_Y = 0.2$ it is clear that the mechanism is sequential for $\lambda' = 0.1$ and 0.3 with
 243 the emergence of dynamically concerted behaviour for larger coupling strengths. However, the fact that

²Note that as discussed previously and shown in Fig. 4, changing the region sizes will lead to some reshuffling of the counts, particularly for those with very large delay times. Nevertheless, the small to moderate time counts and their observed shifts should be robust.

244 there are substantial peaks for $\Delta\tau \gg 10$ does hint at a fairly complex reaction dynamics. Clearly, the most
 245 complex variations in the distribution are seen in Fig. 6 for the $\omega_Y = 0.3$ case. Here, despite the general trend
 246 of the onset of dynamical concerted behaviour with increasing λ' , even for the largest coupling a substantial
 247 fraction of the trajectories exhibit dynamically sequential mechanism. Given the opposing trends in f_{conc}
 248 observed in Fig. 5(a) and (b), one perhaps anticipates the $\lambda \sim \lambda'$ case for lower values of ω_Y to be in a sort
 249 of ‘‘crossover’’ region.

250 It is worthwhile pointing out the following interpretation of the delay time distribution results presented
 251 here. In a given molecular system, characterized by the parameters G and D , the multitude of a_g -symmetry
 252 modes couple with a range of ω_Y, λ , and λ' values. The results in Fig. 6 then suggest that in the full
 253 multidimensional system whether the mechanism is dynamically concerted or sequential depends rather
 254 sensitively on the set of ratios $[(\lambda/\lambda')_1, (\lambda/\lambda')_2, \dots, (\lambda/\lambda')_{n_{ag}}]$, where n_{ag} is the total number of a_g -symmetry
 255 modes in a specific molecule. Clearly, similar criteria should exist for other transverse modes belonging to
 256 different symmetry classes. At the moment there is not much known about the dynamical competition
 257 between two or more low frequency modes with different symmetries. Nevertheless, Fig. 6 does provide a
 258 clue as to why any a priori decision on the mechanism based solely on the static PES features is bound to be
 259 problematic. To this end, in the following section we provide further support by establishing a link between
 260 the phase space manifolds and the delay time distributions.

261 3.4. Phase space viewpoint: Lagrangian descriptors are correlated with delay time distributions

262 A crucial observation, as shown in Appendix B, is that the linear analysis of the index-2 saddle equilib-
 263 rium does not shed any light on the changes in the fraction of concerted trajectories with coupling strengths
 264 shown in Fig. 5. The eigenvalues of the linearized system at the index-2 saddle is independent of the
 265 coupling strengths, λ, λ' . This implies that the competition of concerted vs sequential pathways for initial
 266 conditions launched from the vicinity of the index-2 saddle is inherently mediated by the global phase space
 267 structures. More so, these are global invariant manifolds in the phase space and transport initial conditions
 268 between intermediate and product wells. Thus, differentiating which initial conditions have low delay time,
 269 that is dynamically concerted, and high delay time, that is dynamically sequential.

270 In this study, we use Lagrangian descriptors [71–73] (see Appendix C for details on the method) to
 271 identify the changes in the phase space structures with the changes in the coupling strengths and frequency
 272 of the third mode. In the case of three or more degrees of freedom systems, this method has been used
 273 to detect invariant manifolds and reactive islands [74–76], discovering structure in the nuclear phase space
 274 in nonadiabatic quantum dynamics [77], while there is an increasing number of analysis for one and two
 275 degrees of freedom system with and without dissipation and time dependence. We refer the reader to the
 276 references in the open-source book on Lagrangian descriptors [73]. However, for three degrees of freedom
 277 systems with multiple saddles with varying indices, the use of LD has not been studied carefully and we
 278 present some preliminary discussion of this method.

For the three degrees of freedom system, we define the two dimensional section on the five dimensional energy surface

$$\Sigma_{X_s P_s}^+ = \{(X_s, X_a, Y, P_s, P_a, P_y) \in \mathbb{R}^6 \mid X_a = 0, Y = 0, P_y = 0, \dot{X}_a > 0\} \quad (8)$$

279 to inspect changes in the phase space structures with changes in the coupling strength and frequency of
 280 the third mode. We compute the Lagrangian descriptor for initial conditions on the reactant side ($X_s \leq 0$)
 281 of the section (Eqn. (8)). The integration time used is 10 time units which is almost double the cut-off
 282 time for dynamical concerted ($\Delta\tau_c \sim 5$) pathway. While most studies using the LD method, and supported
 283 by theoretical arguments, tend to choose high integration time, we found that the short integration time
 284 of 10 time units gave sufficient time for the structures to form and did not generate the many intricate

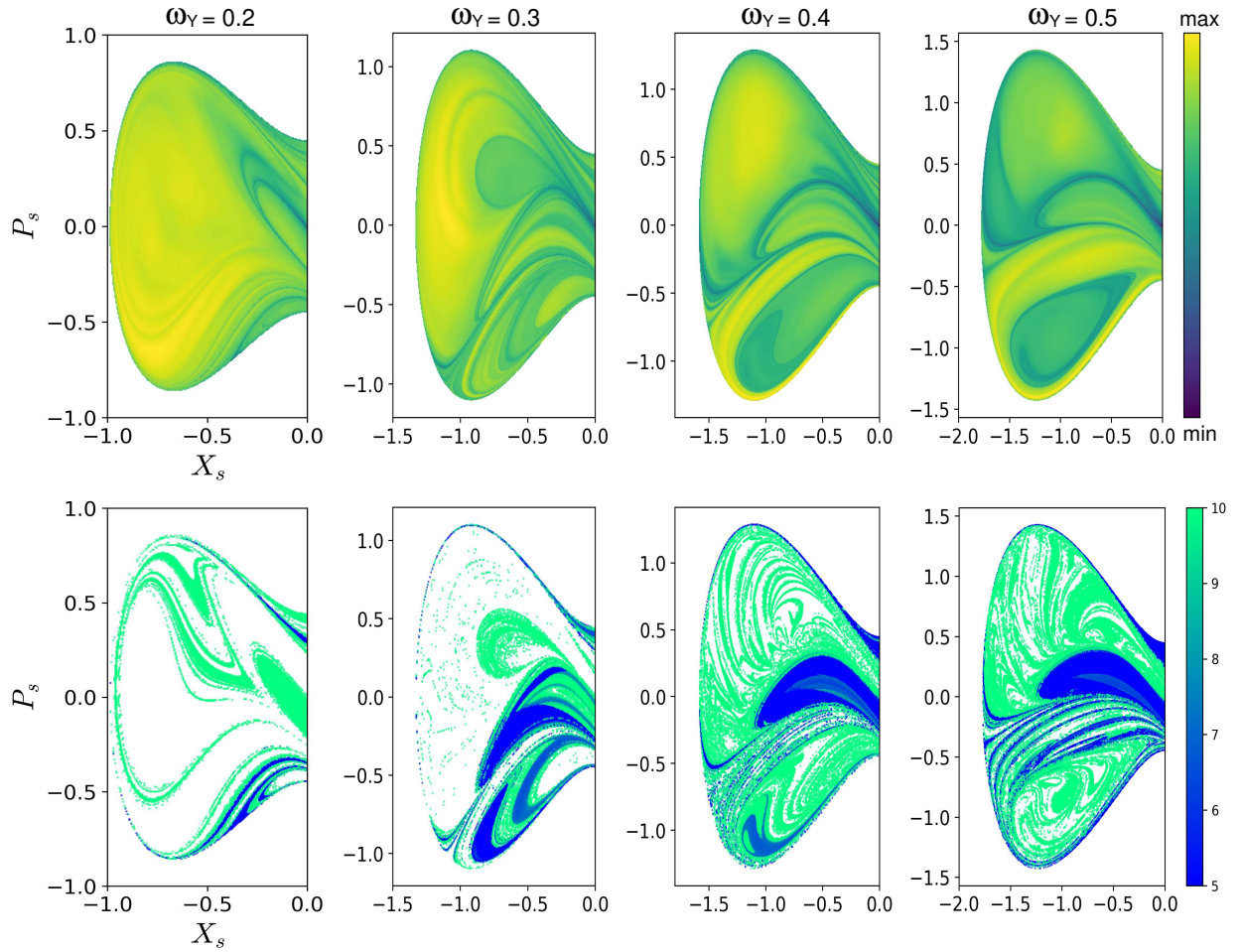


Figure 7: (Top panel) Forward LD map for $\tau = 10$ and (bottom panel) delay time map in the (P_s, X_s) space at total energy of $E = 1.1$. The parameter values are $\lambda = 0.3$, $\lambda' = 0.1$. The frequency ω_Y of the transverse Y-mode is indicated above each column. The color scales associated with LD and delay time map are indicated in the respective panels. Note that the initial conditions of “pure” concerted and dynamically concerted trajectories are shown in blue. The green color indicates the initial condition of trajectories with delay time 10 or greater in the delay time map. The empty (white color) spaces in the delay time map correspond to initial conditions that are non-reactive up to the final time of integration.

285 stretching and folding of the global invariant manifolds. We compare the LD contour map with the delay
286 time map in Figs. 7-9 to show, for the first time, a striking correspondence between the invariant manifolds
287 and delay time distribution. First, we observe that a direct correspondence in the contours of delay times
288 and LD values across all the coupling strengths and frequency of the third mode with a cut-off time for
289 dynamically concerted behaviour of $\Delta\tau_c \sim 5$ time units. The invariant manifolds identified in the LD
290 contour map correspond to initial conditions with high delay time. However, the regions bounded by the
291 invariant manifolds have two distinct delay times, that is either below $\Delta\tau < 5$ or $\Delta\tau > 10$. It implies that the
292 invariant manifolds partition the initial conditions into dynamically concerted or sequential mechanisms.
293 However, it is unclear as to which invariant manifolds can be unambiguously tied to a given mechanism.
294 In order to discern which invariant manifolds mediate dynamically concerted and dynamically sequential
295 mechanisms for energies above the index-2 saddle, one needs to evolve an ensemble of trajectories inside
296 regions bounded by the invariant manifolds. This needs to be paired with a computation of the normally
297 hyperbolic invariant manifolds [78] and its associated global invariant manifolds. The geometry of the
298 normally hyperbolic invariant manifolds (3-sphere) associated with the index-2 saddle and its stable and
299 unstable invariant manifolds (spherical cylinders or with geometry $\mathbb{S}^2 \times \mathbb{R}$) is still an area of continued
300 interest [37, 79, 80] and we expect their structure and stability in the parameter space will shed light on the
301 precise phase space mechanism of the competition between the concerted and sequential pathways.

302 4. Conclusion and Outlook

303 In this work we have studied the classical dynamics of a three degrees of freedom Hamiltonian which
304 models the double proton transfer reaction in a particular class of molecules. However, the analysis and
305 techniques presented here are expected to be relevant for other types of systems which involve breaking and
306 forming of multiple bonds. The key points that emerge from our study are as follows:

- 307 1. Coupling of additional low frequency modes to the reactive modes can lead to a change in the reaction
308 mechanism inferred from lower dimensional studies. In particular, in the context of the DPT reaction
309 studied in this work, it is seen that even a single low frequency mode can substantially change the
310 fraction of reactive trajectories that proceed along the concerted pathway. It would be instructive to
311 construct the phase space dividing surface for the index-2 saddle, along the lines of the earlier work
312 by Collins, Ezra, and Wiggins [80], to gain further insights into the modulation of the fraction of
313 concerted trajectories.
- 314 2. Inspired by several earlier studies on various reactions that involve multiple bond formation, we have
315 explored the utility of classifying reactions as dynamically concerted or sequential. To this end a
316 simple, but dynamical, measure involving the time delay between the formation of two bonds was
317 used. We suggest that the distributions of delay times provides much more information than the
318 fraction of concerted trajectories and its use is motivated by the work of [43]. More importantly, we
319 show a direct correspondence between the delay times and the phase space invariant manifolds for
320 the coupling strengths and frequency of the third mode. This observation, therefore, places the earlier
321 studies on a firm dynamical basis.
- 322 3. We have shown that the technique of Lagrangian descriptors can be invoked to map out the relevant in-
323 variant manifolds in high dimensional phase space. In particular, although not explored further in the
324 current work, we observe that the LDs do encode the manifolds responsible for both the dynamically
325 concerted and the dynamically sequential reactive pathways. Further studies on the changes in the
326 structure of the index-2 normally hyperbolic invariant manifolds (NHIM) [8, 81] with the transverse
327 mode frequency and connection to the LD maps will be the focus of our future work.

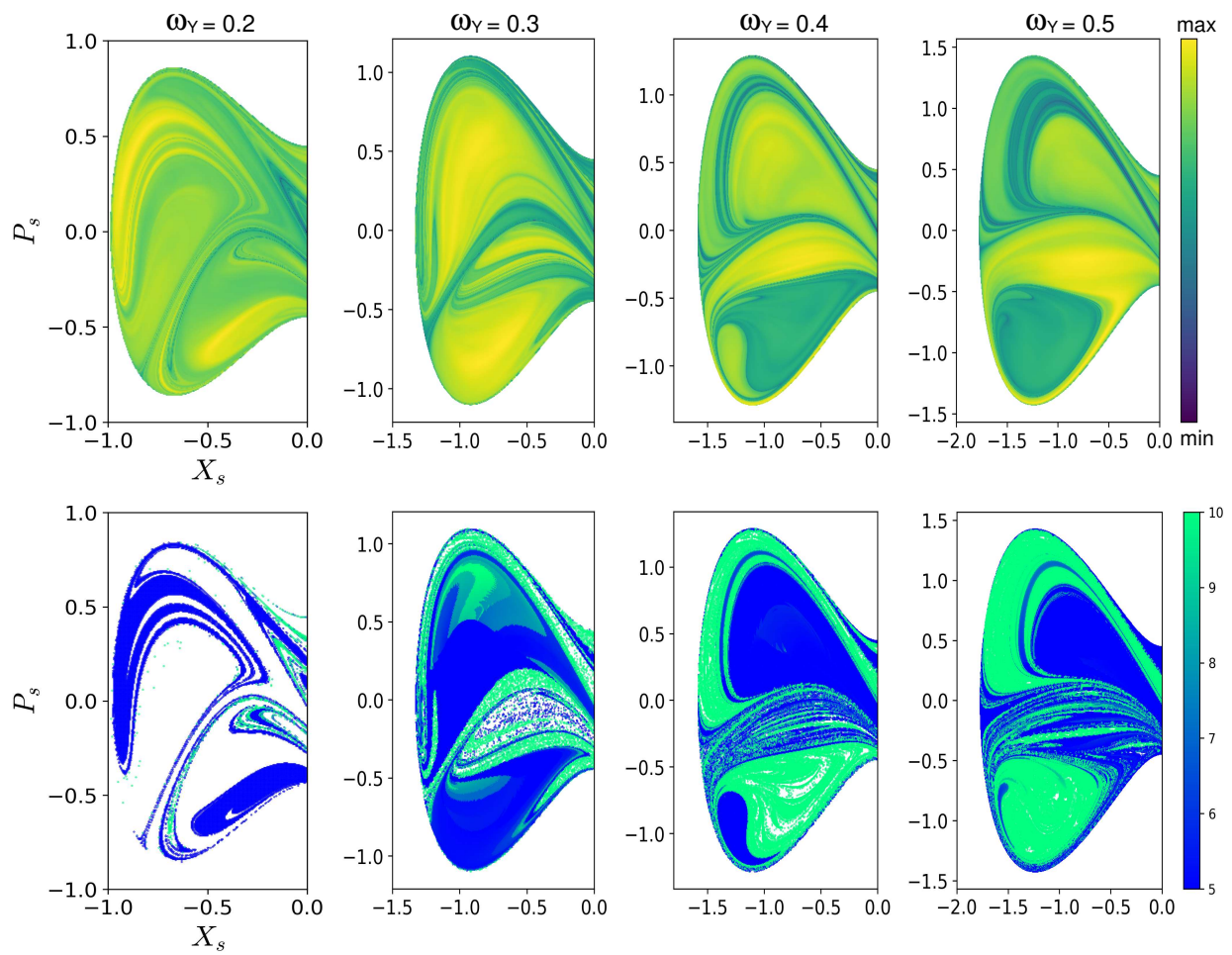


Figure 8: Same as in Fig. 7 with parameter values $\lambda = 0.3$ and $\lambda' = 0.3$.

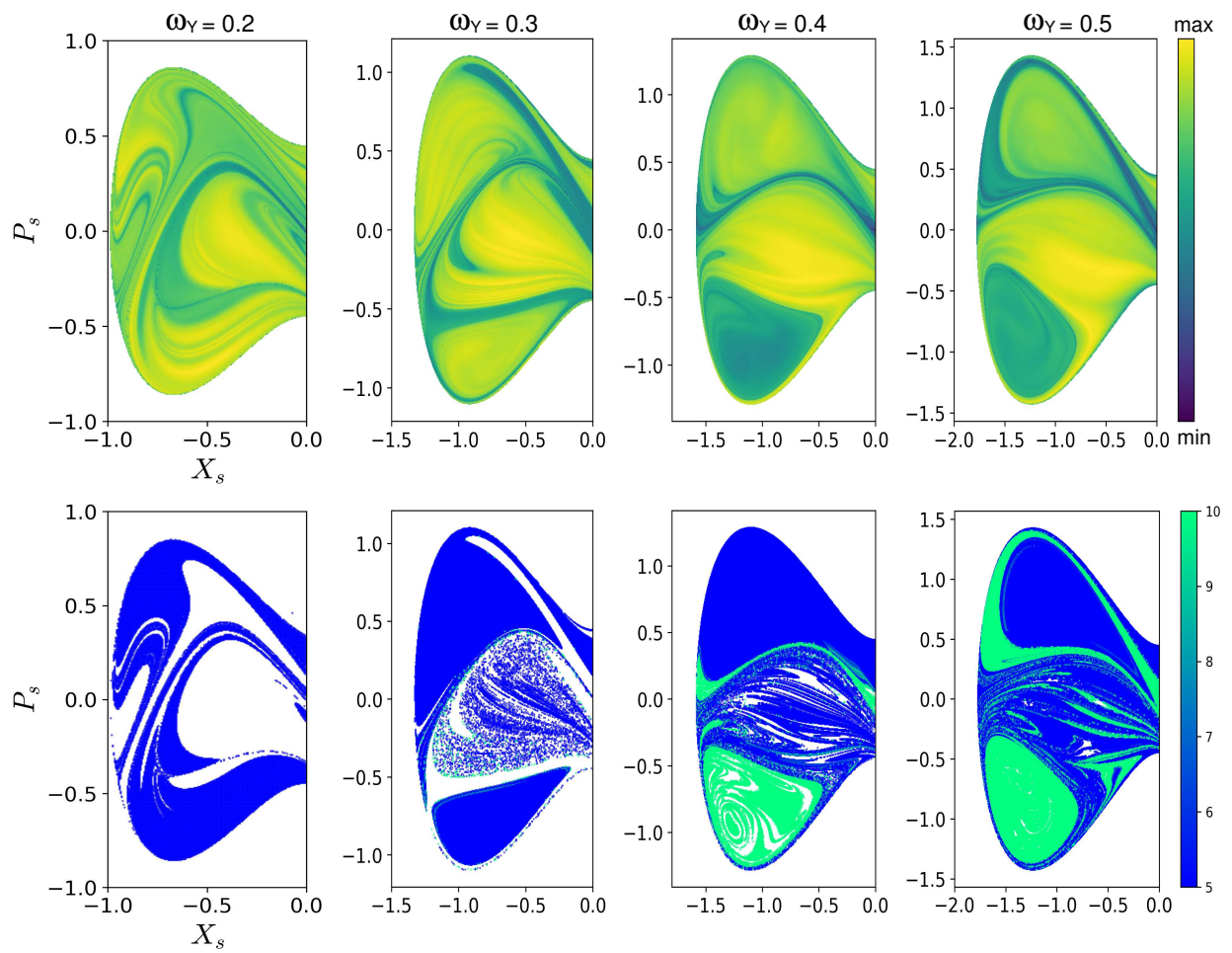


Figure 9: Same as in Fig. 7 with parameter values $\lambda = 0.3$ and $\lambda' = 0.5$.

328 Several issues arise in the context of our, admittedly preliminary, study and we briefly mention a few.
 329 Firstly, are the concerted and sequential pathways uncorrelated? One way to address this is to compute
 330 the so called gap time distribution [17, 82–85] for the model system and the possible connections to the
 331 delay time distributions. Such a connection, along with an unambiguous disentangling of the phase space
 332 invariant manifolds for the two mechanisms, will then allow for decomposing the rate of the reaction in
 333 terms of “concerted rates” and “sequential rates”. Secondly, the extent of intramolecular vibrational energy
 334 redistribution (IVR) [4, 5, 86] amongst the modes needs to be brought out clearly. Since the model has
 335 three degrees of freedom, it would be relevant to map out the Arnold web structure [6, 87, 88] in the
 336 intermediate wells and correlate with the residence time distributions [89]. Such insights from the IVR
 337 dynamics may lead to the identification of the “trigger” modes of the molecule that ultimately result in a
 338 concerted or sequential mechanism. Finally, our entire study is classical and raises the question of whether
 339 the quantum dynamics also allows for a dynamically concerted or sequential classification. The issue is
 340 subtle since, apart from tunneling which is relevant at low temperatures and correlated dynamics due to
 341 quantum entanglement [65], even a proper definition of the delay time may pose difficulties.

342 We conclude by noting that the Hamiltonian in eq. 7 leads to a very rich and complex dynamics. Our
 343 study here has explored only a thin “slice” of the vast parameter range. We hope that a more detailed
 344 phase space analysis and classical-quantum correspondence study of the model presented herein will lead
 345 to further insights into the dynamical implications of high index saddles on reaction mechanisms.

346 5. Acknowledgement

347 We thank Antonio Fernández-Ramos and Zorka Smedarchina for clarifying certain aspects of the po-
 348 tential energy surface used in their various studies of DPT. SK’s research is supported by the Science and
 349 Engineering Research Board (SERB) India (project no. EMR/006246). SN acknowledges the support of
 350 EPSRC Grant No. EP/P021123/1 (CHAMPS project). PP thanks the IIT Kanpur for graduate fellowship
 351 and the High Performance Computing Facility at IIT Kanpur for computing resources.

352 Appendix A. Double proton transfer Hamiltonian: scaled 2D model

For a single proton transfer process, labeled as subsystem 1 in Fig. 1, the standard model corresponds to a quartic double well oscillator with the Hamiltonian

$$\bar{H}(\bar{x}, \bar{p}) = \frac{1}{2\bar{m}}\bar{p}^2 + U(\bar{x}) \quad (\text{A.1})$$

and the potential energy function

$$U(\bar{x}) = -a\bar{x}^2 + b\bar{x}^4 + U_0 \quad (\text{A.2})$$

353 with $\bar{a}, \bar{b} > 0$ and U_0 being the barrier height for the single barrier proton transfer. The critical points of
 354 the potential are determined as $\bar{x}_c = 0, \pm\Delta x_0$ with $\Delta x_0 \equiv (a/2b)^{1/2}$. The point $x_c = 0$ corresponds to the
 355 maximum with $U(0) \equiv U_0 = a^2/4b$ while $x_c = \pm\Delta x_0$ are the two minima with $U(x_c = \pm\Delta x_0) = 0$. Thus,
 356 U_0 is the barrier height. As indicated in Fig. 1, the distance between the two minima is equal to $2\Delta x_0$.

357 We introduce scaled variables as follows. The coordinate is scaled by Δx_0 as $\bar{x} = x\Delta x_0$, with x being
 358 dimensionless. Thus, the potential energy transforms as

$$U(x) = -a(\Delta x_0)^2 x^2 + b(\Delta x_0)^4 x^4 + U_0 \quad (\text{A.3})$$

$$= U_0 [x^2 - 1]^2 \quad (\text{A.4})$$

Consequently, the Hamiltonian can be written down as

$$\bar{H}(x, P) = \frac{(\Delta x_0)^2}{2\bar{m}} P^2 + U_0 [x^2 - 1]^2 \quad (\text{A.5})$$

where $P \equiv \bar{m}\dot{x}$. Measuring mass in units of the proton mass m_H we have $\bar{m} = m_H m$ and $P = \bar{m}\dot{x} = m_H(m\dot{x}) \equiv m_H \tilde{p}$. Finally, scaling the energy by $2U_0$ and time as $t = \alpha\tau$ with $\alpha = [(\Delta x_0)^2 m_H / 2U_0]^{1/2}$ we obtain the transformed dimensionless Hamiltonian

$$H(x, p) = \frac{1}{2m} p^2 + \frac{1}{2} [x^2 - 1]^2 \quad (\text{A.6})$$

359 with the identification $p \equiv m(dx/d\tau)$.

We now consider the double proton transfer scenario shown in Fig. 1 wherein the system has two such equivalent protons tunneling sites. A two degree of freedom Hamiltonian can then be expressed in terms of the two proton coordinates $\mathbf{x} = (x_1, x_2)$ and their corresponding conjugate momenta $\mathbf{p} = (p_1, p_2)$

$$H(\mathbf{x}, \mathbf{p}) = H_0(\mathbf{x}, \mathbf{p}) + U_{\text{coup}}(\mathbf{x}) \quad (\text{A.7})$$

where, the zeroth-order Hamiltonian is generalized from Eqn. A.6 and of the form

$$H_0(\mathbf{x}, \mathbf{p}) = \sum_{j=1,2} \left[\frac{1}{2m_j} p_j^2 + U_0(x_j) \right] \quad (\text{A.8})$$

with

$$U_0(x_j) = \frac{1}{2} [x_j^2 - 1]^2 \quad (\text{A.9})$$

The zeroth-order form is appropriate in the limit that the two protons being transferred are not correlated. However, typically, the two proton motions are coupled and general symmetry-based arguments indicate that the correct form of the coupling potential is given by

$$U_{\text{coup}}(\mathbf{x}) = -2Gx_1x_2 - Dx_1^2x_2^2 - C(x_1^3x_2 + x_1x_2^3) + \dots \quad (\text{A.10})$$

360 Thus, in principle there are couplings of all order between the two modes. However, as has been noted
 361 earlier, from a perturbative perspective the first two leading order terms in the above expansion for $U_{\text{coup}}(\mathbf{x})$
 362 are sufficient to capture most of the essential dynamical features of the system. Therefore, in what follows
 363 we take $G, D \neq 0$ and ignore the higher order terms.

At this stage it is useful to switch from the local coordinates used above to the normal mode coordinates (x_s, x_a) with the transformation $(x_1, x_2) = (x_s + x_a, x_s - x_a)$. The Hamiltonian in this new representation is given by

$$H(x_s, x_a, p_s, p_a) = \frac{1}{2M} (p_s^2 + p_a^2) + \left(\frac{\delta m}{M^2} \right) p_s p_a + U(x_s, x_a) \quad (\text{A.11})$$

with $M \equiv m_1 + m_2$ and $\delta m = m_1 - m_2$. Note the presence of the momentum coupling term. This term vanishes when we are looking at the symmetric $m_1 = m_2$ cases, as in the present work. However, when considering singly substituted isotope case like $m_1 = m_H$ and $m_2 = m_D$, for instance, then $\delta m \neq 0$. The potential thus transforms into

$$U(x_s, x_a) = \alpha_s [x_s^2 - (\Delta x_s)^2]^2 + \alpha_a [x_a^2 - (\Delta x_a)^2]^2 + 2Rx_s^2x_a^2 + \mathcal{U}(G, D) \quad (\text{A.12})$$

where we have denoted $R = 3 + D$ and $\alpha_s = \alpha_a \equiv \alpha = 1 - D$ with

$$\Delta x_{s,a} = \sqrt{\frac{1 \pm G}{1 - D}} \quad (\text{A.13a})$$

$$\mathcal{U}(G, D) = 1 - \alpha_s(\Delta x_s)^4 - \alpha_a(\Delta x_a)^4 \quad (\text{A.13b})$$

As a final transformation, and preparation for the three degree of freedom Hamiltonian of interest to the current work, we transform to mass-weighted coordinates via $X_{s,a} \rightarrow \sqrt{M}x_{s,a}$. We thus obtain the Hamiltonian

$$H(\mathbf{X}, \mathbf{P}) = \frac{1}{2}(P_s^2 + P_a^2) + \left(\frac{\delta m}{M}\right)P_s P_a + U(X_s, X_a) \quad (\text{A.14})$$

with the potential energy term

$$U(\mathbf{X}) = \bar{\alpha}_s \left[X_s^2 - (\Delta X_s)^2 \right]^2 + \bar{\alpha}_a \left[X_a^2 - (\Delta X_a)^2 \right]^2 + 2\bar{R}X_s^2 X_a^2 + \mathcal{U}(G, D) \quad (\text{A.15})$$

364 In the above we have denoted $(\mathbf{X}, \mathbf{P}) \equiv (X_s, X_a, P_s, P_a)$ with the parameters $\Delta X_{s,a} = \sqrt{M}\Delta x_{s,a}$, $\bar{\alpha}_s = \bar{\alpha}_a \equiv$
 365 α/M^2 , and $\bar{R} \equiv R/M^2$. The above Hamiltonian with $\delta m = 0$ corresponds to Eqn. 1 in the main article.

366 Appendix B. Hamiltonian vector field and linear stability of equilibria

367 The Hamiltonian vector field is given by

$$\begin{aligned} \dot{X}_s &= P_s + \frac{\delta m}{M}P_a \\ \dot{X}_a &= P_a + \frac{\delta m}{M}P_s \\ \dot{Y} &= P_y \\ \dot{P}_s &= -4\left(\bar{\alpha}_s(X_s^3 - X_s(\Delta X_s)^2) + \bar{R}X_s X_a^2\right) + 2\lambda X_s \left(Y - \frac{\lambda}{\omega_Y^2}X_s^2 - \frac{\lambda'}{\omega_Y^2}X_a^2 \right) \\ \dot{P}_a &= -4\left(\bar{\alpha}_a(X_a^3 - X_a(\Delta X_a)^2) + \bar{R}X_a X_s^2\right) + 2\lambda' X_a \left(Y - \frac{\lambda}{\omega_Y^2}X_s^2 - \frac{\lambda'}{\omega_Y^2}X_a^2 \right) \\ \dot{P}_y &= -\omega_Y^2 \left(Y - \frac{\lambda}{\omega_Y^2}X_s^2 - \frac{\lambda'}{\omega_Y^2}X_a^2 \right) \end{aligned} \quad (\text{B.1})$$

This vector field has same number of equilibria as the two degrees of freedom model except that each equilibria also has a third coordinate. The equilibria, total energies, and their linear stability is summarised in the Table. 1, where the locations of the index-1 saddles and their energy are given by

$$(X_s^\ddagger, X_a^\ddagger, Y^\ddagger) = \left(\pm \sqrt{\frac{\bar{\alpha}_s \bar{\alpha}_a (\Delta X_s)^2 - \bar{\alpha}_a \bar{R} (\Delta X_a)^2}{(\bar{\alpha}_s \bar{\alpha}_a - \bar{R}^2)}}, \pm \sqrt{\frac{\bar{\alpha}_s \bar{\alpha}_a (\Delta X_a)^2 - \bar{\alpha}_s \bar{R} (\Delta X_s)^2}{(\bar{\alpha}_s \bar{\alpha}_a - \bar{R}^2)}}, \frac{\lambda}{\omega_Y^2} (X_s^\ddagger)^2 + \frac{\lambda'}{\omega_Y^2} (X_a^\ddagger)^2 \right) \quad (\text{B.2})$$

$$H^\ddagger = \frac{1}{M^2(\bar{R}^2 - \bar{\alpha}_a \bar{\alpha}_s)} \left[\bar{R}^2 \bar{\alpha}_s (\Delta X_s)^4 + \bar{R}^2 \bar{\alpha}_a (\Delta X_a)^4 - 2\bar{R}(\Delta X_s \Delta X_a)^2 \bar{\alpha}_s \bar{\alpha}_a \right] + \mathcal{U}(G, D). \quad (\text{B.3})$$

368 The linear stability of the equilibria in Table 1 is determined by the eigenvalue problem associated with
 369 the linearized vector field, $\mathbb{J}\mathbf{v} = \beta\mathbf{v}$, where the Jacobian \mathbb{J} is given by Eqn. (B.4), β, \mathbf{v} are the eigenvalues

370 and eigenvectors of the Jacobian at the equilibrium point. For the reactant, product, and intermediate wells,
 371 the eigenvalues are of the form $\pm\omega_{c1}^e, \pm\omega_{c2}^e, \pm\omega_{c3}^e$. For the saddles at energy H^\ddagger , the eigenvalues are of the
 372 form $\pm\lambda^e, \pm\omega_{s1}^e, \pm\omega_{s2}^e$ which makes these index-1 saddles. For the saddle at energy $E_s = 1$, the eigenvalues
 373 are of the form $\pm\lambda_{s1}^e, \pm\lambda_{s2}^e, \pm\omega_{s3}^e$ which makes this an index-2 saddle.

374 The Jacobian of the vector field, $\mathbb{J}(X_s, X_a, Y, P_s, P_a, P_y)$, is given by

$$\begin{pmatrix} 0 & 0 & 0 & 1 & \frac{\delta m}{M} & 0 \\ 0 & 0 & 0 & \frac{\delta m}{M} & 1 & 0 \\ 0 & 0 & 0 & 0 & 0 & 1 \\ -\frac{\partial^2 V}{\partial X_s^2} & -\frac{\partial^2 V}{\partial X_a \partial X_s} & -\frac{\partial^2 V}{\partial Y \partial X_s} & 0 & 0 & 0 \\ -\frac{\partial^2 V}{\partial X_s \partial X_a} & -\frac{\partial^2 V}{\partial X_a^2} & -\frac{\partial^2 V}{\partial Y \partial X_a} & 0 & 0 & 0 \\ -\frac{\partial^2 V}{\partial X_s \partial Y} & -\frac{\partial^2 V}{\partial X_a \partial Y} & -\frac{\partial^2 V}{\partial Y^2} & 0 & 0 & 0 \end{pmatrix}, \quad (\text{B.4})$$

375 where

$$-\frac{\partial^2 V}{\partial X_s^2} = -4 \left[\bar{\alpha}_s (3X_s^2 - (\Delta X_s)^2) + \bar{R} X_a^2 \right] + 2\lambda \left(Y - \frac{\lambda}{\omega_Y^2} 3X_s^2 - \frac{\lambda'}{\omega_Y^2} X_a^2 \right) \quad (\text{B.5})$$

$$-\frac{\partial^2 V}{\partial X_a^2} = -4 \left[\bar{\alpha}_a (3X_a^2 - (\Delta X_a)^2) + \bar{R} X_s^2 \right] + 2\lambda' \left(Y - \frac{\lambda}{\omega_Y^2} X_s^2 - \frac{\lambda'}{\omega_Y^2} 3X_a^2 \right) \quad (\text{B.6})$$

$$-\frac{\partial^2 V}{\partial X_a \partial X_s} = -\frac{\partial^2 V}{\partial X_s \partial X_a} = -4 \left(2\bar{R} + \frac{\lambda\lambda'}{\omega_Y^2} \right) X_s X_a \quad (\text{B.7})$$

$$-\frac{\partial^2 V}{\partial Y \partial X_s} = -\frac{\partial^2 V}{\partial X_s \partial Y} = 2\lambda X_s \quad (\text{B.8})$$

$$-\frac{\partial^2 V}{\partial Y \partial X_a} = -\frac{\partial^2 V}{\partial X_a \partial Y} = 2\lambda' X_a \quad (\text{B.9})$$

$$-\frac{\partial^2 V}{\partial Y^2} = -\omega_Y^2 \quad (\text{B.10})$$

376 We track the changes in the linear stability of the index-1 and index-2 saddles with changes in the
 377 coupling strength by tracking the eigenvalues of the linearized vector field (Jacobian (B.4)) evaluated at the
 378 equilibrium points as the coupling strength is continuously varied. Note that in this work we have $\delta m = 0$.

The eigenvalues at the phase space point $(0, 0, 0, 0, 0, 0)$ are given by

$$\left[\pm 2 \sqrt{\bar{\alpha}_s} \Delta X_s, \pm 2 \sqrt{\bar{\alpha}_a} \Delta X_a, \pm i\omega_Y \right] \quad (\text{B.11})$$

379 which has the structure of an index-2 saddle and is only dependent on the parameters D, G, C, ω_Y . This
 380 supports the parametric study in this work where the index-2 saddle maintains its linear stability as we vary
 381 λ, λ' . Further, this also points to the fact that mere linear (local in the neighborhood of the equilibrium point)
 382 analysis will not reflect the dynamical mechanism due to the influence of the coupling parameters on the
 383 fraction of concerted trajectories. For the remaining equilibria, we show the changes in the magnitude of the

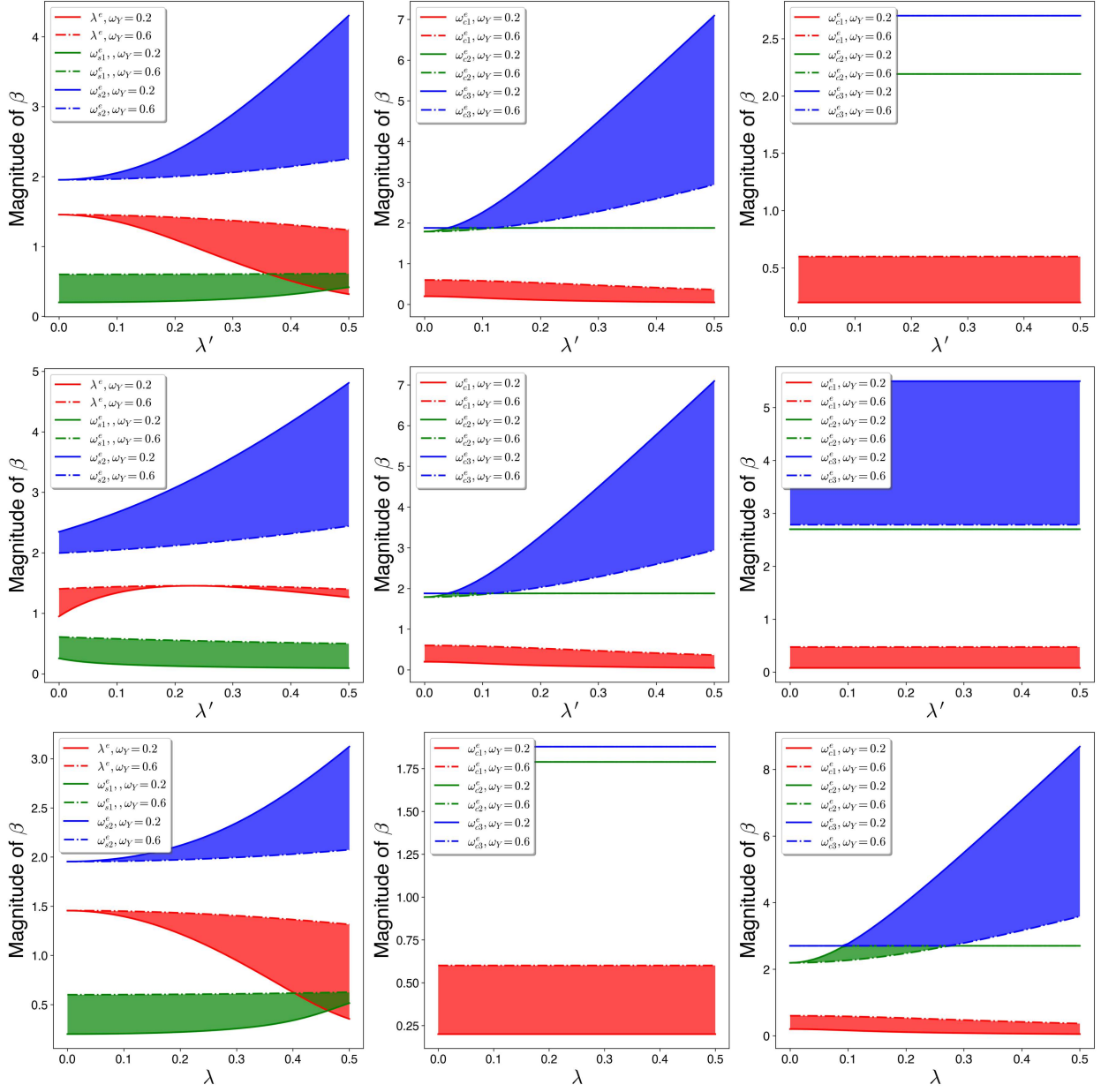


Figure B.10: Eigenvalues variation with λ' , λ , ω_Y . (Top row) $\lambda = 0.0$ (Middle row) $\lambda = 0.3$ (Bottom row) $\lambda' = 0.0$. Left, middle, and right columns correspond to the index-1 saddles, intermediate wells, and product (or reactant) well, respectively. The magnitude of the eigenvalues at $\omega_Y = 0.2$ and $\omega_Y = 0.6$ are shown as continuous line and dash-dot line, respectively, with the shaded region between the lines denoting the variation for $0.2 \leq \omega_Y \leq 0.6$. Other parameters are $\delta M = 0$, $M = 2$, $G = 0.20$, $D = 0.15$.

384 eigenvalues along coupling parameters λ' , λ and third mode frequency ω_Y for $\lambda = 0.3$, $\lambda = 0.0$ and $\lambda' = 0.0$
 385 in Fig. B.10. We observe that the eigenvalues of the intermediate wells are independent of λ while the
 386 eigenvalues of the product (or reactant) well are independent of λ' . In general, there are no critical changes
 387 in the eigenvalues as the coupling strengths and frequency of the third mode are varied. The stability type
 388 of the equilibria stays the same.

389 **Appendix C. Lagrangian descriptor: method to reveal the invariant manifolds**

We briefly describe the method of Lagrangian descriptors, which reveals regions with qualitatively distinct dynamical behavior by showing the intersection of the invariant manifolds with the two dimensional section. For a general time-dependent dynamical system given by

$$\frac{d\mathbf{x}}{dt} = \mathbf{f}(\mathbf{x}, t), \quad \mathbf{x} \in \mathbb{R}^n, \quad t \in \mathbb{R}, \quad (\text{C.1})$$

390 where the vector field $\mathbf{f}(\mathbf{x}, t)$ is assumed to be sufficiently smooth both in space and time. The vector field \mathbf{f}
 391 can be prescribed by an analytical model or given from numerical simulations as a discrete spatio-temporal
 392 data set. For instance, the vector field could represent the velocity field of oceanic or atmospheric currents
 393 obtained from satellite measurements or from the numerical solution of geophysical models. For any initial
 394 condition $\mathbf{x}(t_0) = \mathbf{x}_0$, the system of first order nonlinear differential equations (given in Eqn. (C.1)) has a
 395 unique solution represented by the trajectory that starts from that initial point \mathbf{x}_0 at time t_0 .

In this study, we adopt the LD definition

$$\mathcal{L}_p(\mathbf{x}_0, t_0, \tau) = \int_{t_0-\tau}^{t_0+\tau} \sum_{k=1}^n |f_k(\mathbf{x}(t; \mathbf{x}_0), t)|^p dt, \quad p \in (0, 1] \quad (\text{C.2})$$

where f_k is the k -the component of the vector field, Eqn. (C.1) and use $p = 1/2$. We note that the integral can be split into its forward and backward time parts to detect the intersection of stable and unstable manifolds separately. This relates to finding the escape and entry channels into the potential well. In this study, we keep the forward part of the integral given by

$$\mathcal{L}_p^f(\mathbf{x}_0, t_0, \tau) = \int_{t_0}^{t_0+\tau} \sum_{k=1}^n |f_k(\mathbf{x}(t; \mathbf{x}_0), t)|^p dt \quad (\text{C.3})$$

Although this definition of LD does not have an intuitive physical interpretation as that of the arclength definition [71], it allows for a rigorous proof that the ‘‘singular features’’ (non-differentiable points) in the LD contour map identify intersections with stable and unstable invariant manifolds [72]. Another important aspect of what is known in LD literature as the p -(quasi)norm is that degrees of freedom with relevance in escape/transition (reaction) dynamics can be decomposed and computed. This definition was used to show that the method can be used to successfully detect NHIMs and their stable and unstable manifolds in Hénon-Heiles Hamiltonian [90, 91]. For this system, where both fixed (or variable) integration time is used, it has also been shown that the LD scalar field attains a minimum (or maximum) value along with singularity at the intersections of the stable and unstable manifolds, and given by

$$\mathcal{W}^s(\mathbf{x}_0, t_0) = \operatorname{argmin} \mathcal{L}_p^f(\mathbf{x}_0, t_0, \tau), \quad (\text{C.4})$$

396 where $\mathcal{W}^s(\mathbf{x}_0, t_0)$ are the stable manifolds calculated at time t_0 and argmin denotes the phase space coordi-
 397 nates on the two dimensional section that minimize the scalar field, $\mathcal{L}_p^f(\mathbf{x}_0, t_0, \tau)$, over the integration time,
 398 τ . Thus, the scalar field plotted as a contour map identifies the intersection of the stable manifold with a
 399 two dimensional section. This ability of LD contour map to partition trajectories with different phase space
 400 geometry is shown in the right panel of Fig. C.11 as singular values of LD identify the intersection of the
 401 manifolds with the chosen section.

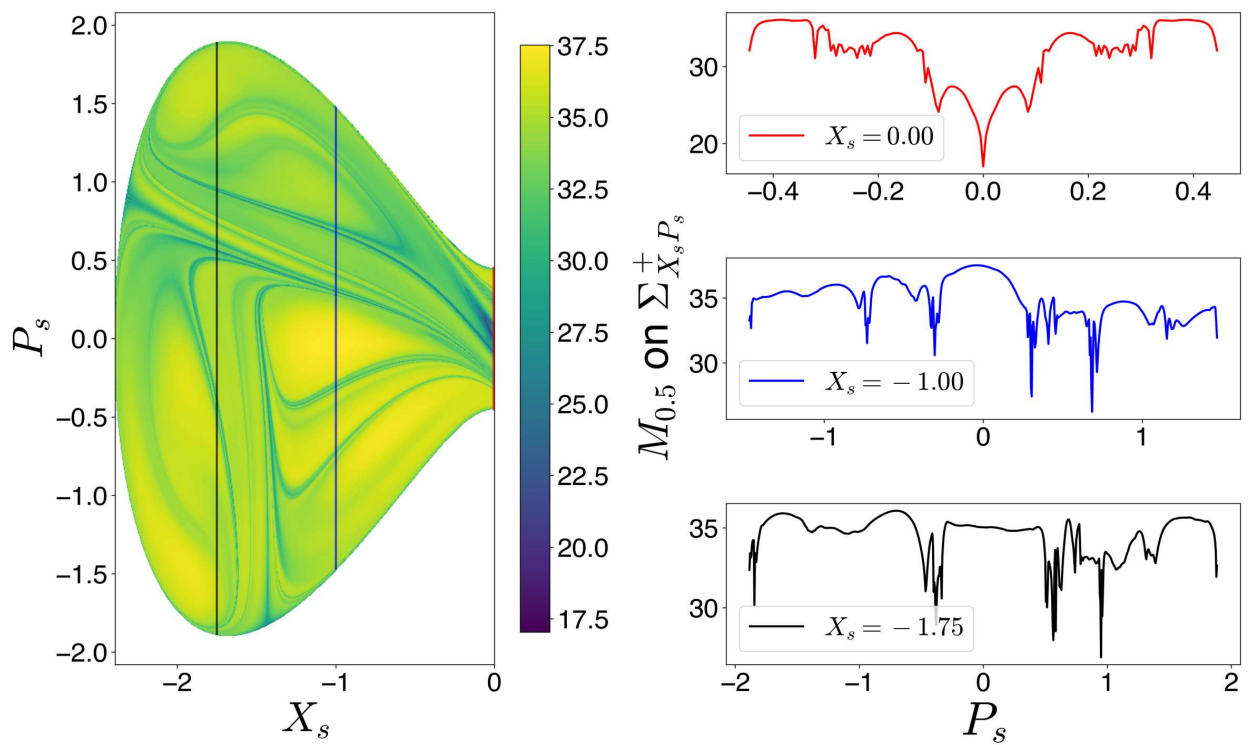


Figure C.11: Lagrangian descriptor (forward) on the section 8 identifying the invariant manifolds by the singular points with minima of the contour map shown by the one dimensional slices on the right. Other parameters are $\lambda = \lambda' = 0, \omega_Y = 0.2$ and $E = 1.1$.

402 References

- 403 [1] T. Uzer, W. Miller, Theories of intramolecular vibrational energy transfer, *Phys. Rep.* 199 (1991) 73–146. doi:10.1016/
404 0370-1573(91)90140-H.
- 405 [2] D. E. Logan, P. G. Wolynes, Quantum localization and energy flow in many-dimensional Fermi resonant systems, *J. Chem.*
406 *Phys.* 93 (1990) 4994–5012. doi:10.1063/1.458637.
- 407 [3] M. Gruebele, Mechanism and control of molecular energy flow: a modeling perspective, *Theor. Chem. Acc.* 109 (2003)
408 53–63. doi:10.1007/s00214-002-0394-2.
- 409 [4] D. M. Leitner, Quantum ergodicity and energy flow in molecules, *Adv. Phys.* 64 (2015) 445–517. doi:10.1080/00018732.
410 2015.1109817.
- 411 [5] S. Keshavamurthy, Scaling perspective on intramolecular vibrational energy flow: Analogies, insights, and challenges, *Adv.*
412 *Chem. Phys.* 153 (2013) 43–110. doi:10.1002/9781118571767.ch2.
- 413 [6] S. Karmakar, S. Keshavamurthy, Intramolecular vibrational energy redistribution and the quantum ergodicity transition: a
414 phase space perspective, *Phys. Chem. Chem. Phys.* 22 (2020) 11139–11173. doi:10.1039/D0CP01413C.
- 415 [7] H. Waalkens, S. Wiggins, Geometrical models of the phase space structures governing reaction dynamics, *Regul. Chaotic*
416 *Dyn.* 15 (2010) 1–39. doi:10.1134/S1560354710010016.
- 417 [8] S. Wiggins, The role of normally hyperbolic invariant manifolds (NHIMS) in the context of the phase space setting for
418 chemical reaction dynamics, *Regul. Chaotic Dyn.* 21 (2016) 621–638. doi:10.1134/S1560354716060034.
- 419 [9] E. Pollak, P. Pechukas, Transition states, trapped trajectories, and classical bound states embedded in the continuum, *J.*
420 *Chem. Phys.* 69 (1978) 1218–1226. doi:10.1063/1.436658.
- 421 [10] P. Pechukas, E. Pollak, Classical transition state theory is exact if the transition state is unique, *J. Chem. Phys.* 71 (1979)
422 2062–2068. doi:10.1063/1.438575.
- 423 [11] H. Waalkens, R. Schubert, S. Wiggins, Wigner’s dynamical transition state theory in phase space: classical and quantum,
424 *Nonlinearity* 21 (2007) R1–R118. doi:10.1088/0951-7715/21/1/r01.
- 425 [12] T. Uzer, C. Jaffé, J. Palacián, P. Yanguas, S. Wiggins, The geometry of reaction dynamics, *Nonlinearity* 15 (2002) 957.
426 doi:10.1088/0951-7715/15/4/301.
- 427 [13] C. Jaffé, S. Kawai, J. Palacián, Y. Patricia, T. Uzer, A new look at the transition state: Wigner’s dynamical perspective
428 revisited, *Adv. Chem. Phys.* 130 (2005) 171–216. doi:10.1002/0471712531.ch3.
- 429 [14] P. Pechukas, Statistical approximations in collision theory, in: *Dynamics of molecular collisions*, Springer, 1976, pp. 269–
430 322. doi:10.1007/978-1-4757-0644-4_6.
- 431 [15] W. H. Miller, Spiers memorial lecture quantum and semiclassical theory of chemical reaction rates, *Faraday Discuss.* 110
432 (1998) 1–21. doi:10.1039/A805196H.
- 433 [16] E. Pollak, P. Talkner, Reaction rate theory: What it was, where is it today, and where is it going?, *Chaos* 15 (2005) 026116.
434 doi:10.1063/1.1858782.
- 435 [17] G. S. Ezra, H. Waalkens, S. Wiggins, Microcanonical rates, gap times, and phase space dividing surfaces, *J. Chem. Phys.*
436 130 (2009) 164118. doi:10.1063/1.3119365.
- 437 [18] P. Collins, G. S. Ezra, S. Wiggins, Phase space structure and dynamics for the Hamiltonian isokinetic thermostat, *J. Chem.*
438 *Phys.* 133 (2010) 014105. doi:10.1063/1.3455712.
- 439 [19] T. Bartsch, R. Hernandez, T. Uzer, Transition state in a noisy environment, *Phys. Rev. Lett.* 95 (2005) 058301. doi:10.1103/
440 *PhysRevLett*.95.058301.
- 441 [20] S. Kawai, T. Komatsuzaki, Dynamic pathways to mediate reactions buried in thermal fluctuations. I. Time-dependent normal
442 form theory for multidimensional Langevin equation, *J. Chem. Phys.* 131 (2009) 224505. doi:10.1063/1.3268621.
- 443 [21] S. Kawai, T. Komatsuzaki, Dynamic pathways to mediate reactions buried in thermal fluctuations. II. Numerical illustrations
444 using a model system, *J. Chem. Phys.* 131 (2009) 224506. doi:10.1063/1.3268622.
- 445 [22] M. Feldmaier, J. Reiff, R. M. Benito, F. Borondo, J. Main, R. Hernandez, Influence of external driving on decays in the
446 geometry of the LiCN isomerization, *J. Chem. Phys.* 153 (2020) 084115. doi:10.1063/5.0015509.
- 447 [23] Ü. Çiftçi, H. Waalkens, Reaction dynamics through kinetic transition states, *Phys. Rev. Lett.* 110 (2013) 233201. doi:10.
448 1103/PhysRevLett.110.233201.
- 449 [24] D. J. Tantillo, *Applied Theoretical Organic Chemistry*, World Scientific, 2018.
- 450 [25] B. K. Carpenter, Trajectories through an intermediate at a fourfold branch point. implications for the stereochemistry of
451 biradical reactions, *J. Am. Chem. Soc.* 107 (1985) 5730–5732. doi:10.1021/ja00306a021.
- 452 [26] B. K. Carpenter, Dynamic matching: The cause of inversion of configuration in the [1, 3] sigmatropic migration?, *J. Am.*
453 *Chem. Soc.* 117 (1995) 6336–6344. doi:10.1021/ja00128a024.
- 454 [27] P. Collins, Z. C. Kramer, B. K. Carpenter, G. S. Ezra, S. Wiggins, Nonstatistical dynamics of the caldera, *J. Chem. Phys.*
455 141 (2014) 034111. doi:10.1063/1.4889780.
- 456 [28] M. Katsanikas, S. Wiggins, Phase space structure and transport in a caldera potential energy surface, *Int. J. Bifurc. Chaos* 28
457 (2018) 1830042. doi:10.1142/S0218127418300422.

- 458 [29] M. Katsanikas, V. J. García-Garrido, S. Wiggins, The dynamical matching mechanism in phase space for caldera-type
459 potential energy surfaces, *Chem. Phys. Lett.* 743 (2020) 137199. doi:10.1016/j.cpllett.2020.137199.
- 460 [30] Y. Geng, M. Katsanikas, M. Agaoglou, S. Wiggins, The influence of a pitchfork bifurcation of the critical points of a
461 symmetric caldera potential energy surface on dynamical matching, *Chem. Phys. Lett.* 768 (2021) 138397. doi:10.1016/j.
462 cpllett.2021.138397.
- 463 [31] J. Rehbein, B. K. Carpenter, Do we fully understand what controls chemical selectivity?, *Phys. Chem. Chem. Phys.* 13
464 (2011) 20906–20922. doi:10.1039/C1CP22565K.
- 465 [32] P. Collins, B. K. Carpenter, G. S. Ezra, S. Wiggins, Nonstatistical dynamics on potentials exhibiting reaction path bifurcations
466 and valley-ridge inflection points, *J. Chem. Phys.* 139 (2013) 154108. doi:10.1063/1.4825155.
- 467 [33] J. B. Thomas, J. R. Waas, M. Harmata, D. A. Singleton, Control elements in dynamically determined selectivity on a
468 bifurcating surface, *J. Am. Chem. Soc.* 130 (2008) 14544–14555. doi:10.1021/ja802577v.
- 469 [34] H. Kurouchi, D. A. Singleton, Labelling and determination of the energy in reactive intermediates in solution enabled by
470 energy-dependent reaction selectivity, *Nat. Chem.* 10 (2018) 237–241. doi:10.1038/nchem.2907.
- 471 [35] H. Kurouchi, I. L. Andujar-De Sanctis, D. A. Singleton, Controlling selectivity by controlling energy partitioning in a thermal
472 reaction in solution, *J. Am. Chem. Soc.* 138 (2016) 14534–14537. doi:10.1021/jacs.6b09052.
- 473 [36] L. M. M. Quijano, D. A. Singleton, Competition between reaction and intramolecular energy redistribution in solution:
474 observation and nature of nonstatistical dynamics in the ozonolysis of vinyl ethers, *J. Am. Chem. Soc.* 133 (2011) 13824–
475 13827. doi:10.1021/ja2043497.
- 476 [37] P. Pandey, S. Naik, S. Keshavamurthy, Classical and quantum dynamical manifestations of index-2 saddles: Concerted versus
477 sequential reaction mechanisms, *Regul. Chaotic Dyn.* 26 (2021) 165–182. doi:10.1134/S1560354721020052.
- 478 [38] H. Teramoto, M. Toda, T. Komatsuzaki, Dynamical switching of a reaction coordinate to carry the system through to a
479 different product state at high energies, *Phys. Rev. Lett.* 106 (2011) 054101. doi:10.1103/PhysRevLett.106.054101.
- 480 [39] A. Accardi, I. Barth, O. Kühn, J. Manz, From synchronous to sequential double proton transfer: Quantum dynamics simula-
481 tions for the model porphine, *J. Phys. Chem. A* 114 (2010) 11252–11262. doi:10.1021/jp103435d.
- 482 [40] E. Goldstein, B. Beno, K. Houk, Density functional theory prediction of the relative energies and isotope effects for the
483 concerted and stepwise mechanisms of the Diels- Alder reaction of butadiene and ethylene, *J. Am. Chem. Soc.* 118 (1996)
484 6036–6043. doi:10.1021/ja9601494.
- 485 [41] H. V. Pham, K. Houk, Diels-Alder reactions of allene with benzene and butadiene: Concerted, stepwise, and ambimodal
486 transition states, *J. Org. Chem.* 79 (2014) 8968–8976. doi:10.1021/jo502041f.
- 487 [42] K. N. Houk, F. Liu, Z. Yang, J. I. Seeman, Evolution of the Diels-Alder reaction mechanism since the 1930s: Woodward,
488 Houk with Woodward, and the influence of computational chemistry on understanding cycloadditions, *Angew. Chem. Int.*
489 *Ed.* 60 (2021) 12660–12681. doi:10.1002/anie.202001654.
- 490 [43] K. Black, P. Liu, L. Xu, C. Doubleday, K. N. Houk, Dynamics, transition states, and timing of bond formation in Diels-Alder
491 reactions, *Proc. Natl. Acad. Sci. U.S.A* 109 (2012) 12860–12865. doi:10.1073/pnas.1209316109.
- 492 [44] S. Takeuchi, T. Tahara, The answer to concerted versus step-wise controversy for the double proton transfer mechanism of
493 7-azaindole dimer in solution, *Proc. Natl. Acad. Sci. U.S.A* 104 (2007) 5285–5290. doi:10.1073/pnas.0610141104.
- 494 [45] H. Ushiyama, K. Takatsuka, Successive mechanism of double-proton transfer in formic acid dimer: A classical study, *J.*
495 *Chem. Phys.* 115 (2001) 5903–5912. doi:10.1063/1.1398090.
- 496 [46] Z. Homayoon, J. M. Bowman, F. A. Evangelista, Calculations of mode-specific tunneling of double-hydrogen transfer in
497 porphycene agree with and illuminate experiment, *J. Phys. Chem. Lett.* 5 (2014) 2723–2727. doi:10.1021/jz501482v.
- 498 [47] M. K. Abdel-Latif, O. Kühn, Laser control of double proton transfer in porphycenes: towards an ultrafast switch for photonic
499 molecular wires, *Theor. Chem. Acc.* 128 (2011) 307–316. doi:10.1007/s00214-010-0847-y.
- 500 [48] M. K. Abdel-Latif, O. Kühn, Infrared laser driven double proton transfer. an optimal control theory study, *Chem. Phys.* 368
501 (2010) 76–82. doi:10.1016/j.chemphys.2009.12.021.
- 502 [49] Y. Nagahata, H. Teramoto, C.-B. Li, S. Kawai, T. Komatsuzaki, Reactivity boundaries for chemical reactions associated with
503 higher-index and multiple saddles, *Phys. Rev. E* 88 (2013) 042923. doi:10.1103/PhysRevE.88.042923.
- 504 [50] R. Pradhan, U. Lourderaj, Can reactions follow non-traditional second-order saddle pathways avoiding transition states?,
505 *Phys. Chem. Chem. Phys.* 21 (2019) 12837–12842. doi:10.1039/C9CP02431J.
- 506 [51] Z. Lu, Y. C. Chang, Q.-Z. Yin, C. Y. Ng, W. M. Jackson, Evidence for direct molecular oxygen production in CO_2 photodis-
507 sociation, *Science* 346 (2014) 61–64. doi:10.1126/science.1257156.
- 508 [52] W. Quapp, J. Maria Bofill, Embedding of the saddle point of index two on the PES of the ring opening of cyclobutene, *Int.*
509 *J. Quantum Chem.* 115 (2015) 1635–1649. doi:10.1002/qua.24996.
- 510 [53] R. Rashmi, K. Yadav, U. Lourderaj, M. Paranjothy, Second-order saddle dynamics in isomerization reaction, *Regul. Chaotic*
511 *Dyn.* 26 (2021) 119–130. doi:10.1134/S1560354721020027.
- 512 [54] F. A. Mauguière, P. Collins, G. S. Ezra, S. C. Farantos, S. Wiggins, Multiple transition states and roaming in ion–molecule
513 reactions: a phase space perspective, *Chem. Phys. Lett.* 592 (2014) 282–287. doi:10.1016/j.cpllett.2013.12.051.

- 514 [55] F. A. Mauguière, P. Collins, Z. C. Kramer, B. K. Carpenter, G. S. Ezra, S. C. Farantos, S. Wiggins, Phase space structures
515 explain hydrogen atom roaming in formaldehyde decomposition, *J. Phys. Chem. Lett.* 6 (2015) 4123–4128. doi:10.1021/
516 acs.jpcllett.5b01930.
- 517 [56] F. A. Mauguière, P. Collins, Z. C. Kramer, B. K. Carpenter, G. S. Ezra, S. C. Farantos, S. Wiggins, Phase space barriers and
518 dividing surfaces in the absence of critical points of the potential energy: Application to roaming in ozone, *J. Chem. Phys.*
519 144 (2016) 054107. doi:10.1063/1.4940798.
- 520 [57] F. A. Mauguière, P. Collins, Z. C. Kramer, B. K. Carpenter, G. S. Ezra, S. C. Farantos, S. Wiggins, Roaming: A phase space
521 perspective, *Annu. Rev. Phys. Chem.* 68 (2017) 499–524. doi:10.1146/annurev-physchem-052516-050613.
- 522 [58] F. G. Montoya, S. Wiggins, Revealing roaming on the double morse potential energy surface with Lagrangian descriptors, *J.*
523 *Phys. A: Math. Theor.* 53 (2020) 235702. doi:10.1088/1751-8121/ab8b75.
- 524 [59] Z. C. Kramer, B. K. Carpenter, G. S. Ezra, S. Wiggins, Reaction path bifurcation in an electrocyclic reaction: ring-opening
525 of the cyclopropyl radical, *J. Phys. Chem. A* 119 (2015) 6611–6630. doi:10.1021/acs.jpca.5b02834.
- 526 [60] Z. Smedarchina, W. Siebrand, A. Fernández-Ramos, Multiple proton transfer: From stepwise to concerted, *Hydrogen-*
527 *Transfer Reactions* (2006) 895–945. doi:10.1002/9783527611546.ch29.
- 528 [61] T. Yoshikawa, S. Sugawara, T. Takayanagi, M. Shiga, M. Tachikawa, Theoretical study on the mechanism of double proton
529 transfer in porphycene by path-integral molecular dynamics simulations, *Chem. Phys. Lett.* 496 (2010) 14–19. doi:10.1016/
530 j.cpllett.2010.07.009.
- 531 [62] T. Yoshikawa, S. Sugawara, T. Takayanagi, M. Shiga, M. Tachikawa, Quantum tautomerization in porphycene and its
532 isotopomers: Path-integral molecular dynamics simulations, *Chem. Phys.* 394 (2012) 46–51. doi:10.1016/j.chemphys.
533 2011.12.007.
- 534 [63] Ł. Walewski, J. Waluk, B. Lesyng, Car-Parrinello molecular dynamics study of the intramolecular vibrational mode-sensitive
535 double proton-transfer mechanisms in porphycene, *J. Phys. Chem. A* 114 (2010) 2313–2318. doi:10.1021/jp907754r.
- 536 [64] Z. Smedarchina, W. Siebrand, A. Fernández-Ramos, Correlated double-proton transfer. I. Theory, *J. Chem. Phys.* 127 (2007)
537 174513. doi:10.1063/1.2785186.
- 538 [65] Z. Smedarchina, W. Siebrand, A. Fernández-Ramos, Entanglement and co-tunneling of two equivalent protons in hydrogen
539 bond pairs, *J. Chem. Phys.* 148 (2018) 102307. doi:10.1063/1.5000681.
- 540 [66] Z. Smedarchina, W. Siebrand, A. Fernández-Ramos, Tunneling splitting in double-proton transfer: Direct diagonalization
541 results for porphycene, *J. Chem. Phys.* 141 (2014) 174312. doi:10.1063/1.4900717.
- 542 [67] Z. Wang, J. S. Hirschi, D. A. Singleton, Recrossing and dynamic matching effects on selectivity in a Diels-Alder reaction,
543 *Angew. Chem. Int. Ed.* 48 (2009) 9156–9159. doi:10.1002/anie.200903293.
- 544 [68] B. Horn, J. Herek, A. Zewail, Retro-Diels-Alder femtosecond reaction dynamics, *J. Am. Chem. Soc.* 118 (1996) 8755–8756.
545 doi:10.1021/ja9620696.
- 546 [69] L. Xu, C. E. Doubleday, K. Houk, Dynamics of 1,3-dipolar cycloadditions: energy partitioning of reactants and quantitation
547 of synchronicity, *J. Am. Chem. Soc.* 132 (2010) 3029–3037. doi:10.1021/ja909372f.
- 548 [70] Z. Yang, C. S. Jamieson, X.-S. Xue, M. Garcia-Borràs, T. Benton, X. Dong, F. Liu, K. Houk, Mechanisms and dynamics of
549 reactions involving entropic intermediates, *Trends Chem.* 1 (2019) 22–34. doi:10.1016/j.trechm.2019.01.009.
- 550 [71] A. M. Mancho, S. Wiggins, J. Curbelo, C. Mendoza, Lagrangian descriptors: A method for revealing phase space structures
551 of general time dependent dynamical systems, *Commun. Nonlinear Sci. Numer. Simul.* 18 (2013) 3530–3557. doi:10.1016/
552 j.cnsns.2013.05.002.
- 553 [72] C. Lopesino, F. Balibrea-Iniesta, V. J. García-Garrido, S. Wiggins, A. M. Mancho, A Theoretical Framework for Lagrangian
554 Descriptors, *Int. J. Bifurcat. Chaos* 27 (2017) 1730001. doi:10.1142/S0218127417300014.
- 555 [73] M. Agaoglu, B. Aguilar-Sanjuan, V. J. García Garrido, F. González-Montoya, M. Katsanikas, V. Krajiňák, S. Naik,
556 S. Wiggins, Lagrangian Descriptors: Discovery and Quantification of Phase Space Structure and Transport, Zenodo,
557 2020. URL: https://champsproject.github.io/lagrangian_descriptors/. doi:10.5281/zenodo.3958985, EP-
558 SRC Grant Number: EP/P021123/1.
- 559 [74] S. Naik, V. J. García-Garrido, S. Wiggins, Finding NHIM: Identifying high dimensional phase space structures in reaction
560 dynamics using Lagrangian descriptors, *Commun. Nonlinear Sci. Numer. Simul.* 79 (2019) 104907. doi:10.1016/j.cnsns.
561 2019.104907.
- 562 [75] S. Naik, S. Wiggins, Finding normally hyperbolic invariant manifolds in two and three degrees of freedom with Hénon-
563 Heiles-type potential, *Phys. Rev. E* 100 (2019) 022204. doi:10.1103/PhysRevE.100.022204.
- 564 [76] S. Naik, S. Wiggins, Detecting reactive islands in a system-bath model of isomerization, *Phys. Chem. Chem. Phys.* 22 (2020)
565 17890–17912. doi:10.1039/DOCP01362E.
- 566 [77] E. C. Eklund, N. Ananth, Investigating the Stability and Accuracy of a Classical Mapping Variable Hamiltonian for Nonadi-
567 abatic Quantum Dynamics, *Regul. Chaotic Dyn.* 26 (2021) 131–146. doi:10.1134/S1560354721020039.
- 568 [78] S. Wiggins, Normally hyperbolic invariant manifolds in dynamical systems., Springer, 2014.
- 569 [79] G. S. Ezra, S. Wiggins, Phase-space geometry and reaction dynamics near index 2 saddles, *J. Phys. A: Math. Theor.* 42

- (2009) 205101. doi:10.1088/1751-8113/42/20/205101.
- 571 [80] P. Collins, G. S. Ezra, S. Wiggins, Index k saddles and dividing surfaces in phase space with applications to isomerization
572 dynamics, *J. Chem Phys.* 134 (2011) 244105. doi:10.1063/1.3602465.
- 573 [81] G. S. Ezra, S. Wiggins, Phase-space geometry and reaction dynamics near index 2 saddles, *J. Phys. A Math. Theor.* 42 (2009)
574 205101. doi:10.1088/1751-8113/42/20/205101.
- 575 [82] N. B. Slater, New formulation of gaseous unimolecular dissociation rates, *J. Chem. Phys.* 24 (1956) 1256–1257. doi:10.
576 1063/1.1742756.
- 577 [83] N. B. Slater, *Theory of unimolecular reactions*, Cornell University Press, 1959.
- 578 [84] E. Thiele, Comparison of the classical theories of unimolecular reactions, *J. Chem Phys.* 36 (1962) 1466–1472. doi:10.
579 1063/1.1732765.
- 580 [85] E. Thiele, Comparison of the classical theories of unimolecular reactions. II. A model calculation, *J. Chem Phys.* 38 (1963)
581 1959–1966. doi:10.1063/1.1733903.
- 582 [86] D. J. Nesbitt, R. W. Field, Vibrational energy flow in highly excited molecules: Role of intramolecular vibrational redistri-
583 bution, *J. Phys. Chem.* 100 (1996) 12735–12756. doi:10.1021/jp960698w.
- 584 [87] S. Karmakar, S. Keshavamurthy, Relevance of the resonance junctions on the Arnold web to dynamical tunneling and
585 eigenstate delocalization, *J. Chem Phys.* 122 (2018) 8636–8649. doi:10.1021/acs.jpca.8b08626.
- 586 [88] S. Karmakar, P. K. Yadav, S. Keshavamurthy, Stable chaos and delayed onset of statisticality in unimolecular dissociation
587 reactions, *Commun. Chem.* 3 (2020) 1–11. doi:10.1038/s42004-019-0252-y.
- 588 [89] A. Shojiguchi, C.-B. Li, T. Komatsuzaki, M. Toda, Fractional behavior in multidimensional Hamiltonian systems describing
589 reactions, *Phys. Rev. E* 76 (2007) 056205. doi:10.1103/PhysRevE.76.056205.
- 590 [90] A. S. Demian, S. Wiggins, Detection of periodic orbits in Hamiltonian systems using Lagrangian descriptors, *Int. J. Bifurcat.*
591 *Chaos* 27 (2017) 1750225. doi:10.1142/S021812741750225X.
- 592 [91] S. Naik, S. Wiggins, Finding normally hyperbolic invariant manifolds in two and three degrees of freedom with Hénon-Heiles
593 type potential, *Phys. Rev. E* 100 (2019) 022204. doi:10.1103/PhysRevE.100.022204.